Simulation of stochastic diffusion via first exit times

Per Lötstedt[1] and Lina Meinecke[1]

[1]Division of Scientific Computing, Department of Information Technology, Uppsala University, Uppsala, Sweden, email: perl@it.uu.se, lina.meinecke@it.uu.se

April 2, 2014

Abstract

In molecular biology it is of interest to simulate diffusion stochastically. In the mesoscopic model we partition a biological cell into voxels in an unstructured mesh. In each voxel the number of molecules is recorded at each time step and molecules can jump between neighboring voxels to model diffusion. The jump rates are computed by discretizing the diffusion equation on the unstructured mesh. If the mesh is of poor quality, due to a complicated cell geometry, standard discretization methods can generate negative jump coefficients, which no longer allows the interpretation as the probability to leave the subvolume. We propose a method based on the mean first exit time of a molecule from a subvolume, which guarantees positive jump coefficients. Two approaches to exit times, a global and a local one, are presented and tested in simulations with diffusion and chemical reactions on meshes of different quality in two dimensions.

1 Introduction

In biochemical networks in cells, molecules diffuse in space and may react with other molecules when they are in the vicinity of each other. This process is often modeled by the reaction-diffusion equations, a system of deterministic partial differential equations (PDEs). This *macroscopic* model describes the evolution of the concentration of the molecules in time and space and is a

good approximation for the behavior in the cell in the limit of large molecule numbers. However, many molecular species of interest in a biological cell, such as the DNA and transcription factors in gene regulation, are present only in very small copy numbers. The law of large numbers is no longer applicable and a deterministic equation for the concentration is inaccurate. We need to simulate the system in a stochastic manner as observed in experiments [10, 34, 37, 39, 43, 46] or is justified theoretically [16, 35]. Diffusion is then modeled as a random walk through space for the molecules and they react with each other with a certain probability when they meet.

One can distinguish at least two levels of modeling for such a random process. The first one is a discrete space, continuous time Markov process for the copy number of the molecules of the chemical species, called the *mesoscopic* model. Here the geometric domain is partitioned into compartments or voxels $\mathcal{V}$ in which the molecules are well mixed. The state of the system is the number of molecules of each species in each voxel. Molecules can then jump between adjacent voxels in diffusion or react with molecules within the same voxel. In a well stirred system, there is no space dependence and a trajectory of the system is generated by the Stochastic Simulation Algorithm (SSA) [18] or more efficient versions of it [5, 17]. The algorithm was extended to problems with spatial variation on Cartesian meshes in [9] implemented in [20] and with curved boundaries in [22] and for unstructured meshes in [11] with software [8, 21]. The second possibility is a continuous space, continuous time Markov process at the more detailed *microscopic* level. Here each individual molecule is tracked and moves by Brownian motion. The molecules react with a certain probability if they are close to each other. Methods and software for this approach are found in [1, 7, 26, 52].

In this paper we focus on the description of diffusion at the mesoscopic level. We will derive the jump coefficients between adjacent voxels for unstructured meshes. Each voxel has a node and the nodes in the mesh are connected by a graph. The time between the jump events is assumed to be exponentially distributed and the jump coefficients are the rates for the jumps from one voxel to the neighboring voxels. These coefficients are determined in [11] by a finite element method (FEM) for the Laplacian Δ and in [21] by a finite volume method (FVM). It follows from [29] that when the number of molecules in the system increases, the concentration of the species will converge to the solution of the diffusion equation discretized in space by FEM or FVM. The jump coefficients depend on the geometry of the mesh and have to be non-negative. For a mesh of poor quality, some of the rates generated by FEM may be negative. The rates generated by a standard FVM are always nonnegative but the coefficients do not always define a consistent discretization of the Laplacian.

The jump rates λ_{ij} from $\mathcal{V}_i$ to $\mathcal{V}_j$ satisfy two conditions

$$1. \quad \lambda_{ij} \geq 0, \qquad 2. \quad \sum_j \lambda_{ij} = \lambda_i, \tag{1}$$

where λ_i is the total jump rate out of $\mathcal{V}_i$. The corresponding approximation of Δu in $\mathcal{V}_i$ on a mesh is then defined by the weights λ_{ij} for the solution values u_j in the neighboring voxels $\mathcal{V}_j$ and $-\lambda_i$ for the value u_i in $\mathcal{V}_i$. The analytical solutions to the Laplace equation or the diffusion equation satisfy a maximum principle. A discrete numerical solution preserving this property satisfies a discrete maximum principle. The same conditions on the coefficients in a discretization of the Laplacian as for the jump rates in (1) are sufficient for the solution to fulfill the discrete maximum principle [49] and the scheme is monotone. The construction of such consistent FEM and FVM for unstructured meshes in 2D and 3D is the subject of a number of papers e.g. [4, 28, 31, 45, 48, 50]. In order for the solution to satisfy the discrete maximum principle there are either geometrical restrictions on the mesh, such as non-obtuse angles, or the coefficients depend on the solution. In [40], non-negativity constraints are added in an optimization problem to assure non-negative solutions of the diffusion equation. Defining a linear scheme for a general unstructured mesh fulfilling (1) with constant coefficients seems to be difficult. Also, to generate a mesh with the angle constraint fulfilled is difficult [2, 12] even in 2D although some progress has been made [13].

We determine λ_{ij} using a different principle. The first exit time of a molecule from a voxel $\mathcal{V}_i$ is the time when a molecule initially inside reaches the boundary $\partial\mathcal{V}_i$ of the voxel and is absorbed there [3, 19, 44]. The jump coefficients are derived from the probability distribution of that time. These coefficients will always be non-negative. The principle is applied locally for the molecules to leave $\mathcal{V}_i$ and globally for them to leave the computational domain Ω. In [36], we compare this approach with FEM, FVM, and the finite difference method (FDM) for Cartesian meshes. The first exit time has been used to improve microscopic simulations with the kinetic Monte Carlo algorithm in [7, 33, 42] and in [47] also in combination with the method in [52].

In the next section, we explain in more detail the mesoscopic algorithm and the problems that are encountered on unstructured meshes. The coefficients are given by discretizations of the Laplacian in Sect. 2. Then we present the theory of first exit times and how it can be used to calculate jump propensities. The numerical experiments with diffusive problems including chemical reactions are reported in Sect. 4. Finally, some conclusions are drawn.

Vectors and matrices are written in boldface. A vector $\mathbf{u}$ has the components u_i and the elements of a matrix $\mathbf{A}$ are A_{ij}. Vectors and matrices are measured in the Euclidean vector norm $\|\mathbf{u}\|$ and its subordinate spectral matrix norm $\|\mathbf{A}\|$.

2 Mesoscopic model for diffusion

In this section, we derive the mesoscopic model for diffusion from a master equation, its mean value equations, and the discretization of the diffusion equation. The spatial domain Ω with boundary $\partial\Omega$ is partitioned into voxels $\mathcal{V}_i,\ i = 1, \ldots, N$, covering the whole domain $\Omega = \bigcup_{i=1}^{N} \mathcal{V}_i$ without overlap between them $\mathcal{V}_i \bigcap \mathcal{V}_j = \emptyset$. Each voxel has a node $\mathbf{x}_i$ inside the boundary $\partial\mathcal{V}_i$ with edges $\mathbf{e}_{ij}$ in a graph connecting $\mathbf{x}_i$ with the node $\mathbf{x}_j$ in the adjacent $\mathcal{V}_j$, see Fig. 1(a). The length, area, or volume of $\mathcal{V}_i$ in 1D, 2D, or 3D, is V_i. The copy number of chemical species Y in $\mathcal{V}_i$ is denoted by y_i. A molecule can jump from $\mathcal{V}_i$ to a $\mathcal{V}_j$ sharing a common part of the boundary $\partial\mathcal{V}_{ij}$ and an edge $\mathbf{e}_{ij}$.

2.1 The master equation

The probability density function (PDF) for a system with only diffusion satisfies a diffusion master equation (DME). The DME is a special case of the chemical master equation with linear reaction propensities [15, Ch. 8], [24, Ch. XIV]. The jump of one molecule of Y from $\mathcal{V}_i$ to $\mathcal{V}_j$ is written as a chemical reaction with the linear propensity v_{ij}

$$Y_i \to Y_j,\ v_{ij}(\mathbf{y}) = \lambda_{ij} y_i. \tag{2}$$

We have a positive λ_{ij} only for cells that are connected by $\mathbf{e}_{ij}$.

The master equation for the PDF $p(\mathbf{y}, t)$ of the diffusion in (2) is

$$\frac{\partial p(\mathbf{y}, t)}{\partial t} = \sum_{i=1}^{N} \sum_{j=1}^{N} \lambda_{ij}(\mathbf{y} - \boldsymbol{\mu}_{ij}) p(\mathbf{y} - \boldsymbol{\mu}_{ij}, t) - \lambda_{ij}(\mathbf{y}) p(\mathbf{y}, t).$$

The transition vector $\boldsymbol{\mu}_{ij}$ is zero except for two components: $\mu_{ij,i} = -1$ and $\mu_{ij,j} = 1$. When there is a jump from $\mathcal{V}_i$ to $\mathcal{V}_j$ then the number of Y decreases by 1 in $\mathcal{V}_i$ ($\mu_{ij,i} = -1$) and the number of Y in $\mathcal{V}_j$ increases by 1 ($\mu_{ij,j} = 1$). All other copy numbers are constant. Molecules in $\mathcal{V}_i$ sharing a part of the boundary $\partial\mathcal{V}_{ib}$ with $\partial\Omega$ cannot jump across $\partial\mathcal{V}_{ib}$ but can jump along $\partial\mathcal{V}_{ib}$.

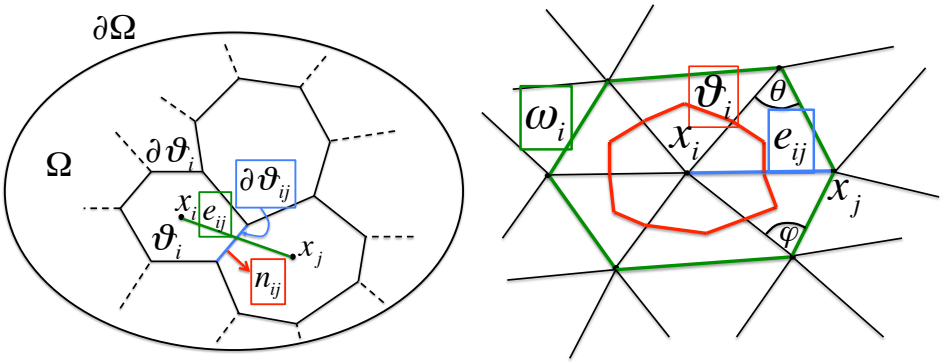

(a) (b)

Fig. 1: (a) Partitioning of Ω into voxels $\mathcal{V}_i$. (b) The primary and secondary mesh with triangles (green and black) and voxels (red) defined by a triangulation.

There is a system of ordinary differential equations (ODEs) for the mean values $\overline{y}_i(t)$ [14, 15, 24]

$$\begin{aligned}\frac{d\overline{y}_i}{dt} &= \sum_{k=1}^{N}\sum_{j=1}^{N}\mu_{kj,i}v_{kj}(\overline{\mathbf{y}}) = \sum_{j=1}^{N}\mu_{ji,i}\lambda_{ji}\overline{y}_j + \sum_{j=1}^{N}\mu_{ij,i}\lambda_{ij}\overline{y}_i \\ &= \sum_{j=1}^{N}\lambda_{ji}\overline{y}_j - \overline{y}_i\sum_{j=1}^{N}\lambda_{ij}, \quad i=1,\ldots,N.\end{aligned} \tag{3}$$

This equation is exact since the propensity v_{kj} is linear. The concentrations of the mean values $c_i = \overline{y}_i/V_i$ satisfy

$$\frac{dc_i}{dt} = \sum_{j=1}^{N}\frac{V_j}{V_i}\lambda_{ji}c_j - c_i\sum_{j=1}^{N}\lambda_{ij}, \quad i=1,\ldots,N. \tag{4}$$

2.2 Discretization of the diffusion equation

At the macroscopic level, the diffusion equation governs the concentrations of the species $\phi(\mathbf{x},t)$

$$\frac{\partial\phi}{\partial t} = \gamma\Delta\phi, \quad \mathbf{x}\in\Omega, \tag{5}$$

with the diffusion coefficient γ. The boundary condition at $\partial\Omega$ with normal $\mathbf{n}$ is a Neumann condition $\mathbf{n}\cdot\nabla\phi = 0$. Discretize the space derivatives by a FEM as in [11] or a FVM on an unstructured mesh defined by the voxels $\mathcal{V}_i$

with a node or vertex $\mathbf{x}_i$ in the center. Let the concentration of the species be ϕ_i in $\mathcal{V}_i$. Then ϕ_i is the solution of the system of ODEs

$$\frac{d\phi_i}{dt} = \sum_{j=1}^{N} \gamma D_{ij}\phi_j = \sum_{j=1, j\neq i}^{N} \gamma D_{ij}\phi_j - \gamma D_{ii}\phi_i, \quad i = 1, \ldots, N, \tag{6}$$

where

$$\mathbf{D} = \mathbf{A}^{-1}\mathbf{S}, \quad D_{ii} = -\sum_{j\neq i} D_{ij}, \quad \mathbf{A} = \mathrm{diag}(A_{ii}). \tag{7}$$

With a FDM on a Cartesian mesh, $\mathbf{A} = \mathbf{I}$ and $\mathbf{S}\boldsymbol{\phi}$ approximates the Laplacian in the voxels. The coefficients on a Cartesian mesh are defined by FDM, FEM, and FVM and compared in [36].

Let the boundary $\partial\mathcal{V}_i$ consist of several straight segments $\partial\mathcal{V}_{ij}, j = 1, \ldots, n_i$, of length $|\partial\mathcal{V}_{ij}|$ with normal $\mathbf{n}_{ij}$ of unit length, see Fig. 1(a). A straightforward finite volume approximation of the Laplacian at $\mathbf{x}_i$ is then

$$\frac{1}{V_i}\int_{\mathcal{V}_i} \Delta\phi \, dv = \frac{1}{V_i}\int_{\partial\mathcal{V}_i} \mathbf{n}\cdot\nabla\phi \, ds \approx \frac{1}{V_i}\sum_{j=1}^{n_i} \mathbf{n}_{ij}\cdot\mathbf{e}_{ij}(\phi_j - \phi_i)\frac{|\partial\mathcal{V}_{ij}|}{\|\mathbf{e}_{ij}\|^2}. \tag{8}$$

In (7), A_{ii} is then equal to V_i and $\mathbf{S}\boldsymbol{\phi}$ approximates the fluxes across $\partial\mathcal{V}_i$. The element $S_{ij} = \mathbf{n}_{ij}\cdot\mathbf{e}_{ij}|\partial\mathcal{V}_{ij}|/\|\mathbf{e}_{ij}\|^2$ in the stiffness matrix is always nonnegative. In a Voronoi mesh, $\mathbf{e}_{ij}$ and $\mathbf{n}_{ij}$ are parallel and the approximation (8) is consistent with $\Delta\phi$, [38]. This is not necessarily the case on a general mesh. Much more complicated coefficients are then needed in 2D [31, 45] depending on the solution ϕ which are difficult to generalize to 3D. The FVM in [21] is cell centered while it is vertex centered in (8).

Linear Lagrangean test and basis functions $\psi_i(\mathbf{x})$ are used in [11] to derive jump coefficients with FEM for the diffusion in a general unstructured mesh defined by a triangles in 2D and by tetrahedra in 3D as in Fig. 1(b). The subdomain ω_i is the union of the triangles or tetrahedra with a corner at $\mathbf{x}_i$. The basis function ψ_i is linear in each triangle or tetrahedron and vansihes outside ω_i. The voxels $\mathcal{V}_i$ consist of the mesh cells in the dual mesh and $\mathcal{V}_i \subset \omega_i$. The matrix $\mathbf{A}$ is defined by mass lumping of the mass matrix $\mathbf{M}$. The components of $\mathbf{A}$ and the stiffness matrix $\mathbf{S}$ are:

$$A_{ii} = V_i, \quad S_{ij} = -\int_{\omega_i} \nabla\psi_i\cdot\nabla\psi_j \, dv, \quad S_{ii} = -\sum_j S_{ij} \leq 0. \tag{9}$$

In 2D,

$$S_{ij} = \sin(\varphi+\theta)/(2\sin(\varphi)\sin(\theta)) \tag{10}$$

where the angles φ and θ are opposing edge $\mathbf{e}_{ij}$ between $\mathbf{x}_i$ and $\mathbf{x}_j$ [50], see Fig. 1(b). If φ and θ are too large such that $\varphi + \theta > \pi$, then $S_{ij} < 0$ and there is no interpretation of S_{ij}/V_i as a conditional probability. A 2D mesh generator usually avoids such angles in the triangles [13] but the condition in 3D on the angles for $S_{ij} \geq 0$ in [50] is more difficult to satisfy in practice [27].

In 1D with the distances Δx_{i-1} and Δx_i between three consecutive nodes x_{i-1}, x_i, and x_{i+1}, the simplest finite difference approximation of u'' is

$$u'' \approx \frac{2}{\Delta x_{i-1}(\Delta x_{i-1} + \Delta x_i)} u_{i-1} - \frac{2}{\Delta x_{i-1}\Delta x_i} u_i + \frac{2}{\Delta x_i(\Delta x_{i-1} + \Delta x_i)} u_{i+1}. \tag{11}$$

The approximation is the same with hat functions as basis and test functions in FEM and in a FVM with a voxel boundary between $\mathcal{V}_{i-1}$ and $\mathcal{V}_i$ at $(x_{i-1} + x_i)/2$ as in [51].

For the concentrations of the mean values c_i in (4) to be equal to the macroscopic concentrations ϕ_i in (6) we let

$$\lambda_{ji} = \gamma \frac{V_i}{V_j} D_{ij} = \gamma \frac{V_i}{V_j} \frac{S_{ij}}{A_{ii}}. \tag{12}$$

In the case of the FVM in (8) and the FEM in (9) the jump coefficient in (1) is

$$\lambda_{ji} = \gamma \frac{S_{ij}}{V_j} = \gamma \frac{S_{ji}}{V_j}, \tag{13}$$

since $\mathbf{S}$ is symmetric.

It seems to be difficult to combine the following properties of a discretization on a general unstructured mesh:

1. Consistency for the Laplacian,
2. The discrete maximum principle,
3. A linear formula,

see e.g. [4, 28, 31, 45, 48, 50]. It is shown in [25] that it is impossible on a quadrilateral mesh in 2D to fulfill all conditions by one scheme. In Section 3, the jump coefficients are obtained from the expected first exit time for a molecule leaving $\mathcal{V}_i$ to $\mathcal{V}_j$.

2.3 The Stochastic Simulation Algorithm

The dimension of the domain of the DME in (3) is the number of voxels N which may be large. Since the diffusion propensity is linear, the analytical

solution can be expressed in convolutions of basic Poisson and multinomial distributions [23] but the solution would be very complicated to compute. Instead, trajectories of the system are generated by the Stochastic Simulation Algorithm (SSA) by Gillespie [18]. The original algorithm was developed for a well stirred system with only reactions. The time to the next reaction is sampled from the cumulative distribution function (CDF) of the exponential distribution. The algorithm is extended to spatially dependent problems with diffusion in the next subvolume mehtod (NSM) [9]. The events in a diffusive system up to the final time T are simulated as follows.

1. Initialize the number of molecules $y_k, k = 1, \ldots, N$, in the N voxels at $t = 0$.

2. Sample the exponentially distributed time t_k with rate $\lambda_k y_k$ to the first diffusion event in all N voxels.

3. Let $i = \text{argmin}\{t_k,\ k = 1, \ldots, N\}$. If $t_i \leq T$ then continue otherwise **stop**.

4. For the jump from $\mathcal{V}_i$, sample a jump to $\mathcal{V}_j$ with probability $\theta_{ij} = \lambda_{ij}/\lambda_i$.

5. Update $t := t_i$, y_i and y_j. Sample Δt_i and Δt_j and recompute $t_i = t + \Delta t_i$ and $t_j = t + \Delta t_j$. Go to 3.

Reactions are included by also introducing reaction events in the voxels with rates depending on the copy numbers in the voxels, see e.g. [9]. The time to the next event is sampled as in step 3 above and the type of event is sampled as in step 4.

3 First exit times

The jump coefficients in (1) are determined by computing the first exit time locally from a subdomain ω of Ω or globally from the whole domain of interest. The total jump rate out of a voxel is then approximated by the inverse of the expected first exit time. The notation is restricted to 2D problems for simplicity but it can easily be extended to 3D.

3.1 General background to first exit times

A molecule moves by Brownian motion and a diffusion constant γ in the domain Ω with boundary $\partial\Omega$. Let T, T_ω, and $\mathbf{X}$ be random variables. The first exit time for the molecule starting at $\mathbf{x}$ in Ω is $T(\mathbf{x})$. Let ω be a

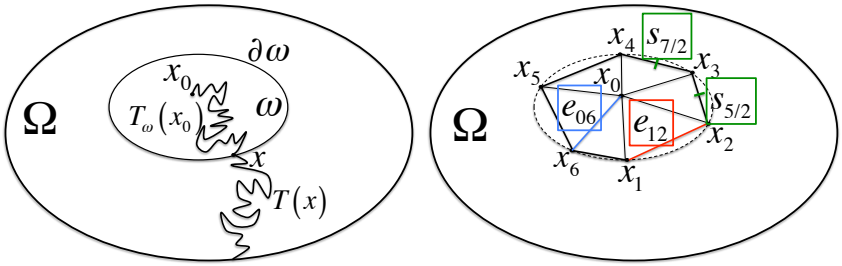

(a) (b)

Fig. 2: (a) Exit times from a subdomain ω and Ω. (b) Discretization of the subdomain ω.

subdomain in Ω, $\omega \subseteq \Omega$, with boundary $\partial\omega$, see Fig. 2(a). The first time for a molecule initially at $\mathbf{x}_0 \in \omega$ at $t = 0$ to reach $\partial\omega$ is $T_\omega(\mathbf{x}_0)$. If the molecule leaves ω at $\mathbf{X}$ then

$$T(\mathbf{x}_0) = T_\omega(\mathbf{x}_0) + T(\mathbf{X}(\mathbf{x}_0)). \tag{14}$$

If $\mathbf{x}_0$ is the initial position in ω then the probability that the molecule exits at $\mathbf{x} \in \partial\omega$ at time t is denoted by $p(\mathbf{x}|\mathbf{x}_0, t) = j(\mathbf{x}, \mathbf{x}_0, t)$. Since $p(\mathbf{x}|\mathbf{x}_0, t)$ is a PDF, we have $\int_{\partial\omega} j(\mathbf{x}(s), \mathbf{x}_0, t)\, ds = 1$, for every $\mathbf{x}_0$ and t. The local exit time PDF from ω starting at $\mathbf{x}_0$ is $p_\omega(t|\mathbf{x}_0)$ and the global exit time PDF out of Ω is $p_\Omega(t|\mathbf{x}_0)$. The expected first exit time from Ω and from ω starting at $\mathbf{x}$ are denoted by $E(\mathbf{x}) = E[T(\mathbf{x})]$ and $e(\mathbf{x}) = E[T_\omega(\mathbf{x})]$, respectively, and the probability to exit ω at $\mathbf{x}$ and t is $p(\mathbf{x}|\mathbf{x}_0, t)p_\omega(t|\mathbf{x}_0)$. Then by conditioning on the first step, the relation between $E(\mathbf{x}_0)$ and $e(\mathbf{x}_0)$ is by (14)

$$\begin{aligned} E(\mathbf{x}_0) &= e(\mathbf{x}_0) + \int_0^\infty \int_0^\infty \int_{\partial\omega} \tau p_\Omega(\tau|\mathbf{x}(s)) p(\mathbf{x}(s)|\mathbf{x}_0, t) p_\omega(t|\mathbf{x}_0)\, ds\, dt\, d\tau \\ &= e(\mathbf{x}_0) + \int_{\partial\omega} \int_0^\infty \tau p_\Omega(\tau|\mathbf{x}(s)) \int_0^\infty j(\mathbf{x}(s), \mathbf{x}_0, t) p_\omega(t|\mathbf{x}_0)\, dt\, d\tau\, ds \\ &= e(\mathbf{x}_0) + \int_{\partial\omega} E(\mathbf{x}(s)) E^s[j(\mathbf{x}(s), \mathbf{x}_0, t)]\, ds, \end{aligned} \tag{15}$$

where $e(\mathbf{x}_0) = \int_0^\infty t p_\omega(t|\mathbf{x}_0)\, dt$ and the coordinate along $\partial\omega$ is $s \in [0, S]$.

To work with discrete meshes we let the boundary $\partial\omega$ be defined by the nodes $\mathbf{x}_i, i = 1, \ldots, n_0$, adjacent to $\mathbf{x}_0$. The nodes can be determined by a triangular mesh in 2D where $\mathbf{x}_0$ and $\mathbf{x}_i$ are connected by an edge $\mathbf{e}_{0i}$. Then a polygonal boundary $\partial\omega$ is obtained by letting $\partial\omega$ consist of the edges $\mathbf{e}_{i,i+1}$ between the nodes $\mathbf{x}_i$ and $\mathbf{x}_{i+1}, i = 1, \ldots, n_0 - 1$, and $\mathbf{e}_{n_0,1}$, see Fig. 2(b) with $n_0 = 6$. If $\partial\omega = \partial\Omega$, then $E(\mathbf{x}(s)) = 0$ and $E(\mathbf{x}_0) = e(\mathbf{x}_0)$.

The integral over $\partial\omega$ in the last expression of (15) is approximated in two different ways. Introduce s_i and $s_{i\pm1/2}$ such that $\mathbf{x}(s_i) = \mathbf{x}_i, \mathbf{x}(s_{i-1/2}) =$

$\frac{1}{2}(\mathbf{x}_{i-1}+\mathbf{x}_i)$, and $\mathbf{x}(s_{i+1/2})=\frac{1}{2}(\mathbf{x}_i+\mathbf{x}_{i+1})$. The expected value $E(\mathbf{x}(s))$ is approximated by $\tilde{E}(\mathbf{x}(s))$ on $\partial\omega$. Either $\tilde{E}$ is constant in an interval or varies linearly there

1. $\tilde{E}_1(\mathbf{x}(s))=\sum_{i=1}^{n_0}E(\mathbf{x}_i)\chi_i(s),\ \chi_i(s)=1, s\in[s_{i-1/2},s_{i+1/2}],\quad \chi_i(s)=0$ otherwise (χ_i is an indicator function),
2. $\tilde{E}_2(\mathbf{x}(s))=\sum_{i=1}^{n_0}E(\mathbf{x}_i)\phi_i(s),\ \phi_i(s_i)=1,\phi_i(s_{i-1})=0,\phi_i(s_{i+1})=0,\ \phi_i$ is linear in $[s_{i-1},s_i]$ and $[s_i,s_{i+1}]$ and 0 otherwise (ϕ_i is a hat function).

Let the temporal mean value of j be

$$\overline{j}_0(\mathbf{x}(s))=E^s[j(\mathbf{x}(s),\mathbf{x}_0,t)]. \tag{16}$$

Then the integral over $\partial\omega$ in (15) is in the first case

$$\begin{aligned}&\int_{\partial\omega}\tilde{E}_1(\mathbf{x}(s))\overline{j}_0(\mathbf{x}(s))\,ds=\int_{\partial\omega}\sum_{i=1}^{n_0}E(\mathbf{x}_i)\chi_i(s)\overline{j}_0(\mathbf{x}(s))\,ds\\&=\sum_{i=1}^{n_0}E(\mathbf{x}_i)\int_{s_{i-1/2}}^{s_{i+1/2}}\overline{j}_0(\mathbf{x}(s))\,ds=\sum_{i=1}^{n_0}E(\mathbf{x}_i)\overline{j}_{0i},\\&\overline{j}_{0i}=\int_{s_{i-1/2}}^{s_{i+1/2}}\overline{j}_0(\mathbf{x}(s))\,ds.\end{aligned} \tag{17}$$

An interpretation of $\overline{j}_{0i}$ is that it is the probability to exit through the section $\partial\omega_i=[s_{i-1/2},x_i,s_{i+1/2}]$ of $\partial\omega=\bigcup_{j=1}^{n_0}\partial\omega_j$, see Fig. 2(b). With the second approximation $\tilde{E}_2$, the integral is

$$\begin{aligned}&\int_{\partial\omega}\tilde{E}_2(\mathbf{x}(s))\overline{j}_0(\mathbf{x}(s))\,ds=\int_{\partial\omega}\sum_{i=1}^{n_0}E(\mathbf{x}_i)\phi_i(s)\overline{j}_0(\mathbf{x}(s))\,ds\\&=\sum_{i=1}^{n}E(\mathbf{x}_i)\int_{s_{i-1}}^{s_{i+1}}\phi_i(s)\overline{j}_0(\mathbf{x}(s))\,ds=\sum_{i=1}^{n}E(\mathbf{x}_i)\overline{j}_{0i},\\&\overline{j}_{0i}=\int_{s_{i-1}}^{s_{i+1}}\phi_i(s)\overline{j}_0(\mathbf{x}(s))\,ds.\end{aligned} \tag{18}$$

The error ε in the approximation with $\tilde{E}_1$ and $\tilde{E}_2$ in (17) and (18) compared to the last integral in (15) is

$$\varepsilon=\int_{\partial\omega}(E(\mathbf{x}(s))-\tilde{E}_k(\mathbf{x}(s)))\overline{j}_0(\mathbf{x}(s))\,ds,\quad k=1,2. \tag{19}$$

The error in (19) with $\tilde{E}_1$ is of $\mathcal{O}(\Delta s)$ if Δs is the maximum length of an interval $[s_{i-1/2},s_{i+1/2}]$. This is shown in the following way. Since $E(\mathbf{x}(s))$

and $j(\mathbf{x}(s), \mathbf{x}_0, t)$ are continuous on $\partial\omega$ but in general have a jump in the derivative along s at the corners $\mathbf{x}(s_i) = \mathbf{x}_i$ of $\partial\omega$, the integral between s_i and the end point $s_{i+1/2}$ can be written

$$\begin{aligned}&\int_{s_i}^{s_{i+1/2}} E(\mathbf{x}(s))\overline{j}_0(\mathbf{x}(s))\,ds \\ &= E(\mathbf{x}_i)\int_{s_i}^{s_{i+1/2}} \overline{j}_0(\mathbf{x}(s))\,ds + E'_{i+}\int_{s_i}^{s_{i+1/2}} (s-s_i)\overline{j}_0(\mathbf{x}(s))\,ds + \mathcal{O}\left(\Delta s^3\right).\end{aligned} \tag{20}$$

The derivatives of $E(\mathbf{x}(s))$ to the left and right of s_i are denoted by E'_{i-} and E'_{i+}, respectively. A bound on the contribution to the error term in (17) from $[s_i, s_{i+1/2}]$ is then to leading order

$$\left|E'_{i+}\int_{s_i}^{s_{i+1/2}} (s-s_i)\overline{j}_0(\mathbf{x}(s))\,ds\right| \le |E'_{i+}| \max_{s\in[s_i,s_{i+1/2}]} \overline{j}_0(\mathbf{x}(s))(s_{i+1/2}-s_i)^2/2. \tag{21}$$

A similar bound is valid for the interval $[s_{i-1/2}, s_i]$. Since

$$|\varepsilon| \le \max_{s\in[0,S]} \overline{j}_0(\mathbf{x}(s)) \sum_{i=1}^{n} \max\{|E'_{i-}|, |E'_{i+}|\}\Delta s^2 \le C_1 \Delta s,$$

ε is bounded by $C_1\Delta s$ where C_1 depends on $E(\mathbf{x})$, j, and the length of $\partial\omega$.

In the second case, $E(\mathbf{x}(s))$ is approximated by linear interpolation in $[s_{i-1}, s_i]$ and $[s_i, s_{i+1}]$ in (18). If $\mathbf{x}(s)$ is a straight line in the intervals then $E(\mathbf{x})$ is smooth. Due to the interpolation error [6, Ch. 7.4.2] to leading order in Δs we have in each one of the subintervals

$$\begin{aligned}&\left|\int_{s_i}^{s_{i+1}} (E(\mathbf{x}(s)) - \tilde{E}_2(\mathbf{x}(s)))\overline{j}_0(\mathbf{x}(s))\,ds\right| \\ &\le \frac{1}{2}|E''_i|\left|\int_{s_i}^{s_{i+1}} (s-s_i)(s-s_{i+1})\overline{j}_0(\mathbf{x}(s))\,ds\right| \le \frac{1}{12}|E''_i| \max_{s\in[s_i,s_{i+1}]} \overline{j}_0(\mathbf{x}(s))\Delta s^3,\end{aligned} \tag{22}$$

where E''_i is a second derivative of $E(\mathbf{x})$ in the interval. Hence, there is also a C_2 such that ε is bounded by $C_2\Delta s^2$ when the approximation with $\tilde{E}_2$ is used.

With the discretization of the functions on $\partial\omega$, the approximations in (17) and (18), and the notation $E_i = E(\mathbf{x}_i)$ and $e_0 = e(\mathbf{x}_0)$, the numerical approximation of the relation between the expected values in (15) is

$$E_0 = e_0 + \sum_{i=1}^{n_0} \overline{j}_{0i} E_i. \tag{23}$$

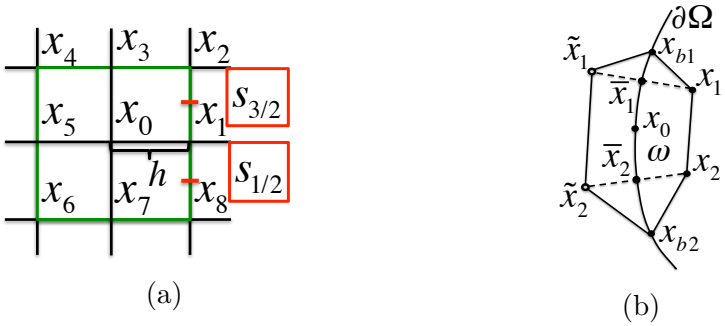

Fig. 3: (a) Cartesian mesh and ω. (b) Boundary treatment.

Note that the conditional probability $\bar{j}_{0i}$ is scaled such that the sum is 1

$$\sum_{i=1}^{n_0} \bar{j}_{0i} = \int_{\partial\omega} \bar{j}_0(\mathbf{x}(s))\, ds = \int_{\partial\omega} E^s[j(\mathbf{x}(s), \mathbf{x}_0, t)\, ds] = E^s[1] = 1. \tag{24}$$

The PDE satisfied by $E(\mathbf{x})$ on a connected domain Ω is [41, Ch. 9]

$$\begin{aligned} \gamma \Delta E(\mathbf{x}) &= -1, \quad \mathbf{x} \in \Omega, \\ E(\mathbf{x}) &= 0, \quad \mathbf{x} \in \partial\Omega. \end{aligned} \tag{25}$$

In 1D, the solution is

$$E(x) = \frac{1}{2\gamma} x(1-x), \quad x \in \Omega = [0,1]. \tag{26}$$

Rearrange the terms in (23) as

$$\sum_{i=1}^{n_0} \frac{\bar{j}_{0i}}{e_0} E_i - \frac{1}{e_0} E_0 = \sum_{i=1}^{n_0} \frac{\bar{j}_{0i}}{e_0} (E_i - E_0) = -1, \tag{27}$$

and interpret (27) as a discretization of (25) at $\mathbf{x}_0$ in Ω. As the jump propensity from the node x_0, λ_0 is the inverse of the expected time e_0 and the coefficients to reach a neighboring node are:

$$\lambda_{0i} = \bar{j}_{0i}/e_0 = \bar{j}_{0i}\lambda_0, \tag{28}$$

compare (13). By using different approximation techniques to numerically solve (25) on different meshes covering Ω, we will arrive at different coefficients λ_0 and $\bar{j}_{0i}$ as in Sect. 2.2.

On an equidistant Cartesian mesh in 2D with square voxels ω in [36], the boundary $\partial\omega$ is defined by $\mathbf{x}_i$, $i = 1, \ldots, 8$, with the step length h between

$\mathbf{x}_i$, see Fig. 3(a). The jump coefficient λ_0 in [36] agrees with the rate from a FDM which is second order accurate. The coordinates $s_{1/2}$ and $s_{3/2}$ defining $\partial\omega_1$ around the midpoint $\mathbf{x}_1 = (x_{11}, x_{12})$ in (17) are chosen to be

$$s_{3/2} = x_{12} + \beta h, \quad s_{1/2} = x_{12} - \beta h, \quad \beta \in [0, 1]. \tag{29}$$

The other intervals $\partial\omega_3, \partial\omega_5$, and $\partial\omega_7$ are defined similarly and $\partial\omega_2, \partial\omega_4, \partial\omega_6$, and $\partial\omega_8$ are the complementary intervals associated with the corners $\mathbf{x}_2, \mathbf{x}_4, \mathbf{x}_6$, and $\mathbf{x}_8$. We have to choose $\beta = 0.56$ for the first exit time approach to correspond to a second order FDM approximation of the Laplacian, resulting in:

$$\overline{j}_{0i} = \int_{s_i - \frac{1}{2}}^{s_i + \frac{1}{2}} \overline{j}_{0i}(\mathbf{x}(s))ds = 0.2053, \quad i = 1, 3, 5, 7. \tag{30}$$

The $\overline{j}_{0i}$ with the hat function in (18) is 0.1629 for $i = 1, 3, 5, 7$. Since using hat functions does not give the coefficients of second order accuracy for the discretization of the diffusion equation we choose $\overline{j}_{0i} = \int_{s_i - \frac{1}{2}}^{s_i + \frac{1}{2}} \overline{j}_{0i}(\mathbf{x}(s))ds$ as in (17) in the remaining sections. The standard five point FDM stencil yields $\lambda_0 = 4\gamma/h^2$, $\overline{j}_{0i} = 1/4$, $i = 1, 3, 5, 7$, and $\overline{j}_{0i} = 0$, $i = 2, 4, 6, 8$.

3.2 Local first exit time

We now want to compute the local exit time to leave ω and $\overline{j}_{0i}$. The probability density is $c(\mathbf{x}, \mathbf{x}_0, t)$ to find a random walker located inside an infinitesimal area at $\mathbf{x}$ in ω at time t given that he started at $\mathbf{x}_0$ at $t = 0$ and has not yet left ω. The mean value of the first exit time e_0 and the jump probabilities $\overline{j}_{0i}$ in (23) can be computed directly from c in ω. The PDE satisfied by c in ω is [44]

$$\begin{aligned} \frac{\partial c(\mathbf{x}, \mathbf{x}_0, t)}{\partial t} &= \gamma \Delta c(\mathbf{x}, \mathbf{x}_0, t), \quad \mathbf{x} \in \omega, \\ c(\mathbf{x}, \mathbf{x}_0, t) = 0, \ \mathbf{x} \in \partial\omega, &\quad c(\mathbf{x}, \mathbf{x}_0, 0) = \delta(\mathbf{x} - \mathbf{x}_0). \end{aligned} \tag{31}$$

The solution is non-negative by the maximum principle and $\mathbf{n} \cdot \nabla c \leq 0$ at $\partial\omega$ with the normal $\mathbf{n}$ directed outward from ω.

When $c > 0$ in ω, then there is a probability that the molecule has survived in ω and not reached the boundary, [7]. The survival probability for a molecule initially at $\mathbf{x}_0$ is

$$S(t) = \int_\omega c(\mathbf{x}, \mathbf{x}_0, t)\, d\omega = P(T_\omega(\mathbf{x}_0) \geq t), \tag{32}$$

which is the probability for the walker to exit at a time greater than t. The CDF of T_ω is $1 - S(t)$. Hence the PDF for a molecule to exit at time t is given by (31) and Gauss' formula

$$p_\omega(t|\mathbf{x}_0) = -\frac{\partial S(t)}{\partial t} = -\int_\omega \gamma \Delta c \, d\omega = -\gamma \int_{\partial\omega} \mathbf{n} \cdot \nabla c \, ds \geq 0. \tag{33}$$

Since $\partial S(t)/\partial t \leq 0$ and $S(0) = 1$, the survival probability decays monotonically as t increases. Furthermore, the expected value e_0 of the exit time is obtained from p_ω

$$e_0 = \int_0^\infty t p_\omega(t|\mathbf{x}_0) \, dt = \int_0^\infty S(t) \, dt. \tag{34}$$

Analytical solutions of (31) on ω are known only in special cases. For a general ω, e_0 is obtained from an accurate numerical solution of (31).

Interpreting $-\gamma \nabla c \cdot \mathbf{n}$ as the flux out of the volume ω, the conditional probability that the molecule leaves ω at $\mathbf{x}$ given that the time is t is

$$j(\mathbf{x}, \mathbf{x}_0, t) = \frac{-\gamma \mathbf{n} \cdot \nabla c(\mathbf{x}, \mathbf{x}_0, t)}{p_\omega(t|\mathbf{x}_0)} = \frac{\mathbf{n} \cdot \nabla c(\mathbf{x}, \mathbf{x}_0, t)}{\int_{\partial\omega} \mathbf{n} \cdot \nabla c(\mathbf{x}(s), \mathbf{x}_0, t) \, ds}, \tag{35}$$

and consequently, the probability for the molecule to exit along the edge $\partial\omega_i$ is

$$j_i(\mathbf{x}_0, t) = \int_{\partial\omega_i} j(\mathbf{x}(s), \mathbf{x}_0, t) \, ds = \frac{\int_{\partial\omega_i} \mathbf{n} \cdot \nabla c(\mathbf{x}(s), \mathbf{x}_0, t) \, ds}{\int_{\partial\omega} \mathbf{n} \cdot \nabla c(\mathbf{x}(s), \mathbf{x}_0, t) \, ds}. \tag{36}$$

Solving (31) and computing e_0 in (34) and the expected relative coefficients $\overline{j}_{0i}$ as $E[j_i(\mathbf{x}_0, t)]$ in (36) (and also in (17)) is an alternative way of determining the parameters in (23).

A standard unstructured mesh generator to discretize space will generate nodes $\mathbf{x}_i$ which are connected by edges $\mathbf{e}_{ij}$. A straightforward $\partial\omega$ consists of line segments in 2D and flat faces in 3D defined by the nodes adjacent to the center node in ω. Then ω is a polygon in 2D and a volume bounded by polygonal surfaces in 3D. In 1D, $\partial\omega$ is two points x_{i-1} and x_{i+1} and

$$j_{i\pm1}(x_0, t) = \frac{\pm c_x(x_{i\pm1}, x_0, t)}{c_x(x_{i+1}, x_0, t) - c_x(x_{i-1}, x_0, t)}, \quad c_x = \frac{\partial c}{\partial x}. \tag{37}$$

If $\mathbf{x}_0 \in \partial\Omega$, then its ω is constructed by adding new nodes outside Ω for simulation of reflection boundary conditions for the molecules. For each node $\mathbf{x}_i, i = 1, \ldots, n_{0\mathcal{I}}$, in the interior of Ω and connected to $\mathbf{x}_0$ by an edge, a node $\widetilde{\mathbf{x}}_i$ is created by reflection in $\partial\Omega$ such that $\widetilde{\mathbf{x}}_i - \mathbf{x}_i$ is orthogonal to the

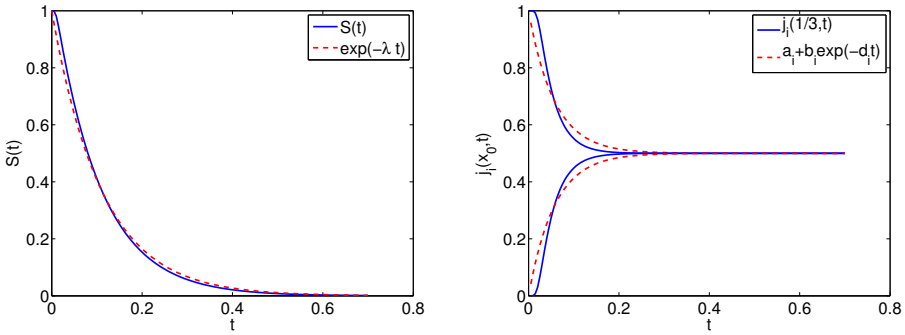

(a) (b)

Fig. 4: First exit time properties on the interval $[0, 1]$ with $\gamma = 1$ and $x_0 = \frac{1}{3}$. (a) $S(t)$, (b) $j_i(x_0, t)$ and their exponential approximations.

boundary at $\bar{\mathbf{x}}_i = \frac{1}{2}(\widetilde{\mathbf{x}}_i + \mathbf{x}_i) \in \partial\Omega$, and $\|\mathbf{x}_i - \bar{\mathbf{x}}_i\| = \|\widetilde{\mathbf{x}}_i - \bar{\mathbf{x}}_i\|$. Then ω is defined by $\mathbf{x}_i, \widetilde{\mathbf{x}}_i, i = 1, \ldots, n_{0\mathcal{I}}$, and the two nodes $\mathbf{x}_{b1}, \mathbf{x}_{b2}$, on $\partial\Omega$ adjacent to $\mathbf{x}_0$, see Fig. 3(b). The jump coefficients are computed as in a ω but the conditional probability $\overline{j}_{0i}$ for a jump to an exterior node $\widetilde{\mathbf{x}}_i$ is added to $\overline{j}_{0i}$ of the corresponding interior node $\mathbf{x}_i$. This is how reflection in the boundary is achieved for a diffusing molecule.

In order to obtain a continuous-time Markov chain, we assume that the first exit time for a molecule leaving ω via $\partial\omega_i$ is exponentially distributed with rate λ_{0i}. Then

$$\tilde{p}_{\omega_i}(t|\mathbf{x}_0) = \lambda_{0i} \exp(-\lambda_{0i} t). \tag{38}$$

The total rate to exit ω is then $\lambda_0 = \sum_i^n \lambda_{0i}$ and the exit time T_ω from ω is also exponentially distributed with

$$\tilde{p}_{\omega}(t|\mathbf{x}_0) = \lambda_{0} \exp(-\lambda_{0} t). \tag{39}$$

Hence, by (33) and (34) we arrive at

$$\tilde{S}(t) = \exp(-\lambda_0 t), \;\; e_0 = 1/\lambda_0. \tag{40}$$

The rate λ_{0i} to leave at node i is related to e_0 and $\overline{j}_{0i}$ by $\lambda_{0i} = \overline{j}_{0i}/e_0 = \overline{j}_{0i}\lambda_0$, cf. (28). The typical behavior of $S(t)$ and $j_i(\mathbf{x}_0, t)$ is found for a 1D problem in Fig. 4. Here, $S(t)$ is well approximated by a $\tilde{S}(t)$.

Also $j_i(\mathbf{x}_0, t)$ can be approximated by a sum including an exponential, see Fig. 4(b). Suppose that

$$j_i(\mathbf{x}_0, t) = a_i + b_i \exp(-d_i t). \tag{41}$$

Then the conditional probability $\bar{j}_{0i}$ in (17) and (18) satisifes

$$\frac{\lambda_{0i}}{\lambda_0} = \bar{j}_{0i} = \int_0^\infty (a_i + b_i \exp(-d_i t))\tilde{p}_\omega(t|\mathbf{x}_0)\, dt = a_i + b_i \frac{1}{1 + d_i/\lambda_0}, \qquad (42)$$

with the approximations in (39) and (41).

The rate λ_0 can be computed in different ways from a numerical solution of (31). Discretize (31) in time and on a mesh covering ω using e.g. a FEM and solve for c. Integrate c as in (32) to obtain $S_k = S(t_k)$ at time points $t_k, k = 0, 1, \ldots, K$, with $t_0 = 0$ and $t_k = t_{k-1} + \Delta t$ for t_K sufficiently large. Then λ_0 is determined using the trapezoidal rule in (34), the linear least squares method on the logarithm of (40), or nonlinear least squares directly on (40)

1. $\lambda_0^{-1} = \int_0^\infty S(t)\, dt \Rightarrow \lambda_0^{-1} = \frac{\Delta t}{2} S_0 + \sum_{k=1}^{K-1} \Delta t S_k + \frac{\Delta t}{2} S_K$,
2. $\lambda_0 t_k \approx -\log S_k \Rightarrow \lambda_0 = -\sum_{k=0}^K t_k \log S_k / \sum_{k=0}^K t_k^2$,
3. $g(\lambda) = \sum_{k=0}^K (\exp(-\lambda t_k) - S_k)^2 \Rightarrow \lambda_0 = \operatorname{argmin}\, g(\lambda)$.

The approximations of $\bar{j}_{0i}$ are obtained in the same manner. Compute $j_{0i}(t_k) = j_i(\mathbf{x}_0, t_k)$ using c with a quadrature formula in (36). Let $a_i = j_{0i}(t_K)$ and $b_i = j_{0i}(t_0) - a_i$. Then d_i is calculated by fitting $\exp(-d_i t_k)$ to $(j_{0i}(t_k) - a_i)/b_i$ using linear or nonlinear least squares as above.

With $\omega = [x_{i-1}, x_{i+1}] = [0, h(1+\kappa)]$, $\kappa > 0$, and $x_i = h$ in 1D, the space step to the left is h and κh to the right of x_i. The solution to (31) with $x_0 = x_i$ is

$$c(x,t) = \sum_{n=1}^\infty \frac{2}{h(1+\kappa)} \sin\left(\frac{n\pi}{1+\kappa}\right) \sin\left(\frac{n\pi x}{h(1+\kappa)}\right) \exp\left(-\frac{n^2\pi^2\gamma t}{h^2(1+\kappa)^2}\right), \qquad (43)$$

the survival probability in (32) is

$$S(t) = \sum_{j=1}^\infty \frac{4}{(2j-1)\pi} \sin\left(\frac{(2j-1)\pi}{1+\kappa}\right) \exp\left(-\frac{(2j-1)^2\pi^2\gamma t}{h^2(1+\kappa)^2}\right), \qquad (44)$$

and the expected exit time from ω in (34) is

$$e_i = \frac{4h^2(1+\kappa)^2}{\pi^3\gamma} \sum_{j=1}^\infty \frac{1}{(2j-1)^3} \sin\left(\frac{(2j-1)\pi}{1+\kappa}\right). \qquad (45)$$

In the same manner the expected relative coefficients $\bar{j}_{i,i\pm1}$ are computed from (37). Then we have

$$e_i = \frac{1}{\lambda_i} = \frac{h^2\kappa}{2\gamma}, \quad \bar{j}_{i,i-1} = \frac{\lambda_{i,i-1}}{\lambda_i} = \frac{\kappa}{1+\kappa}, \quad \bar{j}_{i,i+1} = \frac{\lambda_{i,i+1}}{\lambda_i} = \frac{1}{1+\kappa}. \qquad (46)$$

These coefficients are the same as those derived from the finite difference formula in (11), cf. [3, Ch. 16.5], [11, p. 1780].

3.3 Global first exit time

Another possibility to determine the diffusion jump rates is to use the triangular mesh in 2D or a tetrahedral mesh in 3D on Ω and solve (25) with Dirichlet boundary conditions for E by the FEM on that mesh with linear Lagrangean basis functions $\psi_i(\mathbf{x})$ as in Sect. 2.2. The subvolume ω_i surrounding the node $\mathbf{x}_i$ as in Sect. 3.2 is where $\psi_i \neq 0$. There at $\mathbf{x}_i$ the solution E_i satisfies the discretization (27). Compared to the analytical solution $E(\mathbf{x})$ of (25), the error in E_i is of $\mathcal{O}(\Delta s^2)$ where Δs is the maximum length of an edge in the mesh. Let $\alpha_{ij} = \gamma S_{ij}/V_i$ be derived by applying Neumann conditions at $\partial\Omega$ and use that $\int_\Omega \psi_i \, d\Omega = \int_{\omega_i} \psi_i \, d\Omega = V_i$. Assume that $\mathbf{x}_i$ is connected by edges to n_i vertices $\mathbf{x}_j$, that $i \in \mathcal{I}$ if the node is in the interior of Ω and that $i \in \mathcal{B}$ if $\mathbf{x}_i \in \partial\Omega$. The set of all nodes is $\mathcal{N} = \{1, \ldots, N\} = \mathcal{I} \cup \mathcal{B}$. If $\mathbf{x}_i$ is in the interior of Ω then we have

$$\sum_{j=1}^{n_i} \alpha_{ij}(E_j - E_i) = -1, \quad i \in \mathcal{I}. \tag{47}$$

If $i \in \mathcal{B}$ then there is no relation (47) for E_j but the coefficients α_{ij} are defined by the Neumann condition at $\partial\Omega$ and

$$\sum_{j=1}^{n_i} \alpha_{ij}(E_j - E_i) = \sum_{j=1}^{n_i} \alpha_{ij} E_j = \eta_i, \quad i \in \mathcal{B}, \tag{48}$$

since $E_i = 0$ if $i \in \mathcal{B}$, see (25). If $\alpha_{ij} \geq 0$ and the discrete maximum principle is satisfied at $\partial\Omega$, then $E_j > 0$ and we have $\eta_i > 0$ for $i \in \mathcal{B}$.

Some of the α-coefficients may be negative if the mesh is of insufficient quality. In this case, we choose λ_{ij} close to α_{ij} satisfying (47) in the interior, (48) on the boundary and $\lambda_{ij} \geq 0$. If the coefficients α_{ij} are non-negative we use them as the jump coefficients. This is accomplished by letting λ_{ij} solve the quadratic programming (QP) problem for each node $\mathbf{x}_i$, $i \in \mathcal{N}$,

$$\begin{array}{ll} \min_{\lambda_{ij}} & \sum_{j=1}^{n_i} (\lambda_{ij} - \alpha_{ij})^2, \\ & \sum_{j=1}^{n_i} \lambda_{ij}(E_j - E_i) = \eta_i, \\ & \lambda_{ij} \geq 0, \ j = 1, \ldots, n_i, \end{array} \tag{49}$$

where $\eta_i = -1$ for $i \in \mathcal{I}$. The equality constraint is such that, locally at $\mathbf{x}_i$, the numerical approximation of (15) in (27) is satisfied. Using the vectors

$\boldsymbol{\lambda}, \boldsymbol{\alpha}$, and $\boldsymbol{\beta}$ with $\beta_j = E_j - E_i$, the equivalent QP problem is

$$\begin{array}{ll} \min_{\boldsymbol{\lambda}} & \boldsymbol{\lambda}^T\boldsymbol{\lambda} - 2\boldsymbol{\alpha}^T\boldsymbol{\lambda}, \\ & \boldsymbol{\beta}^T\boldsymbol{\lambda} = \eta_i, \\ & \boldsymbol{\lambda} \geq 0. \end{array} \tag{50}$$

If $\mathbf{u} \geq 0$ for a general vector $\mathbf{u}$, then all components are non-negative. If $\boldsymbol{\alpha} \geq 0$ then $\boldsymbol{\lambda} = \boldsymbol{\alpha}$ is the solution of (49) or (50) since both the minimum of the objective function is achieved and the constraints are satisfied.

An alternative to solve (50) is to choose the simpler QP problem

$$\begin{array}{ll} \min_{\boldsymbol{\mu}} & \boldsymbol{\mu}^T\boldsymbol{\mu} - 2\boldsymbol{\alpha}^T\boldsymbol{\mu}, \\ & \boldsymbol{\mu} \geq 0. \end{array} \tag{51}$$

The optimal solution in (51) is

$$\mu_j = \max(\alpha_j, 0). \tag{52}$$

The solution is non-negative and is the choice in [11]. One small QP problem in (50) or (51) is solved for every node $\mathbf{x}_i$ to find the jump coefficients λ_{ij} there.

The λ-coefficients are determined in (50) by an orthogonal projection of $\boldsymbol{\alpha}$ on the subspace defined by the equality and the non-negativity constraints. The equality constraint is added in the interior of Ω to ensure that taking $\boldsymbol{\lambda}$ as the coefficients in a discretization of the Laplacian yields a good approximation for the global exit time problem in (25) but regarded as such a discretization it is in general not consistent if some $\alpha_j < 0$.

The constraint set $\mathcal{F}_i = \{\boldsymbol{\lambda} | \boldsymbol{\beta}^T\boldsymbol{\lambda} = \eta_i, \ \boldsymbol{\lambda} \geq 0\}$ in (50) is convex and polyhedral and the objective function is bounded from below. Hence, if $\mathcal{F}_i \neq \emptyset$ then the QP problem has a unique solution.

In order to investigate if the feasible set $\mathcal{F}_i$ is empty or not consider two cases with $\eta_i < 0$ and $\eta_i > 0$. If $\eta_i < 0$ e.g. for $i \in \mathcal{I}$ and there is at least one $\beta_k = E_k - E_i < 0$, then there is one positive $\lambda_k = \eta_i/\beta_k$ and $\mathcal{F}_i$ is not empty. On the other hand, if $i \in \mathcal{I}$ and $\boldsymbol{\beta} \geq 0$ then there is no feasible solution. This is possible in spite of $\boldsymbol{\alpha}^T\boldsymbol{\beta} = -1$ in (47) if at least one $\alpha_k < 0$. If $\boldsymbol{\beta} \geq 0$ then E_i is a local minimum and the solution is not satisfying the discrete maximum principle. Let $i \in \mathcal{B}$ with $\eta_i > 0$. Then there is a $\boldsymbol{\lambda} \geq 0$ and $\mathcal{F}_i \neq \emptyset$ if and only if at least one $\beta_k > 0$, i.e. $E_k > 0$ and the discrete maximum principle holds at least locally since $E_i = 0$. The case with $\eta_i < 0$ and $i \in \mathcal{B}$ is treated in the same way as for $i \in \mathcal{I}$ above. If $\mathcal{F}_i = \emptyset$ then the rate coefficients are chosen as in (51) without the equality constraint to ensure that a λ is always found.

By adding the inequality constraints on $\boldsymbol{\mu}$ in (51) the difference between $\boldsymbol{\mu}$ and $\boldsymbol{\alpha}$ is the vector $\delta\boldsymbol{\mu}$ with elements $\delta\mu_j = \mu_j - \alpha_j = |\min(0, \alpha_j)|$. When the equality constraint is added on $\boldsymbol{\lambda}$ in (50) a bound for the difference $\|\boldsymbol{\lambda} - \boldsymbol{\mu}\|$ is derived in the following proposition.

Proposition. *Assume that $\mathcal{F}_i \neq \emptyset$. Let the solutions to* (50) *and* (51) *be $\boldsymbol{\lambda}$ and $\boldsymbol{\mu}$. Introduce the sets $\mathcal{J}_1 = \{j|\lambda_j = 0\}, \mathcal{J}_2 = \{j|\mu_j = 0\}$, and $\mathcal{J} = \mathcal{J}_1 \cup \mathcal{J}_2$ with k elements in $\mathcal{J}$. The n elements in $\boldsymbol{\beta}$ are ordered such that the k components in $\mathcal{J}$ appear first in $\boldsymbol{\beta}$ such that*

$$\boldsymbol{\beta} = \begin{pmatrix} \boldsymbol{\beta}_k \\ \boldsymbol{\beta}_{n-k} \end{pmatrix}, \ \boldsymbol{\beta}_k \in \mathbb{R}^k, \ \boldsymbol{\beta}_{n-k} \in \mathbb{R}^{n-k}.$$

Assume that $k < n$ and $\boldsymbol{\beta}_{n-k} \neq 0$. Then the difference between $\boldsymbol{\lambda}$ solving the QP with the additional equality constraint and $\boldsymbol{\mu}$ is

$$\|\boldsymbol{\lambda} - \boldsymbol{\mu}\| \leq \left(1 + \frac{\|\boldsymbol{\beta}_k\|}{\|\boldsymbol{\beta}_{n-k}\|}\right) \|\boldsymbol{\delta}\|. \tag{53}$$

where

$$\delta_i = |\min(0, \alpha_i)|.$$

Proof. The solution $\boldsymbol{\mu} = \boldsymbol{\alpha} + \boldsymbol{\delta}$ also satisfies

$$\begin{array}{ll} \min_{\boldsymbol{\mu}} & \boldsymbol{\mu}^T\boldsymbol{\mu} - 2\boldsymbol{\alpha}^T\boldsymbol{\mu}, \\ & \boldsymbol{\beta}^T\boldsymbol{\mu} = \boldsymbol{\beta}^T\boldsymbol{\alpha} + \boldsymbol{\beta}^T\boldsymbol{\delta} = \eta + \boldsymbol{\beta}^T\boldsymbol{\delta}, \\ & \boldsymbol{\mu} \geq 0. \end{array} \tag{54}$$

We will compare the solutions to (50) and (54) using [32].

Introduce $\mathbf{D}_0 \in \mathbb{R}^{(k+1)\times n}$, $\mathbf{d}_0 \in \mathbb{R}^{k+1}$, and the identity matrix $\mathbf{I}_k \in \mathbb{R}^{k\times k}$ in

$$\mathbf{D}_0 = \begin{pmatrix} \mathbf{I}_k & 0 \\ \boldsymbol{\beta}_k^T & \boldsymbol{\beta}_{n-k}^T \end{pmatrix}, \ \mathbf{d}_0 = \begin{pmatrix} 0 \\ -\boldsymbol{\beta}^T\boldsymbol{\delta} \end{pmatrix}.$$

If $\boldsymbol{\beta}_{n-k} \neq 0$ then $\mathbf{D}_0$ has full row rank and its generalized inverse $\mathbf{D}_0^+$ and $\mathbf{D}_0^+\mathbf{d}_0$ are defined by

$$\mathbf{D}_0^+ = \mathbf{D}_0^T(\mathbf{D}_0\mathbf{D}_0^T)^{-1} = \begin{pmatrix} \mathbf{I}_k & 0 \\ -\xi\boldsymbol{\beta}_{n-k}\boldsymbol{\beta}_k^T & \xi\boldsymbol{\beta}_{n-k} \end{pmatrix}, \ \mathbf{D}_0^+\mathbf{d}_0 = \begin{pmatrix} 0 \\ -\xi\boldsymbol{\beta}_{n-k}\boldsymbol{\beta}^T\boldsymbol{\delta} \end{pmatrix},$$

with $\xi = 1/\|\boldsymbol{\beta}_{n-k}\|^2$. Then using (3.4) and (3.11) in [32] we conclude that

$$\|\boldsymbol{\lambda} - \boldsymbol{\mu}\| \leq \|\mathbf{D}_0^+\mathbf{d}_0\| = \xi|\boldsymbol{\beta}^T\boldsymbol{\delta}|\|\boldsymbol{\beta}_{n-k}\| = \frac{|\boldsymbol{\beta}^T\boldsymbol{\delta}|}{\|\boldsymbol{\beta}_{n-k}\|} \leq \left(1 + \frac{\|\boldsymbol{\beta}_k\|}{\|\boldsymbol{\beta}_{n-k}\|}\right) \|\boldsymbol{\delta}\|,$$

and the proposition is proved. ■

Remark 1. It follows from the proposition that when $k = 0$ then $\boldsymbol{\lambda} = \boldsymbol{\mu}$, i.e. the equality constraint has not changed the solution and $\boldsymbol{\alpha} = \boldsymbol{\lambda} = \boldsymbol{\mu}$. The most common case is that k is small, e.g. $k = 1$. Then $\|\boldsymbol{\beta}_k\|/\|\boldsymbol{\beta}_{n-k}\|$ is often small and the change in the solution is approximately $\|\boldsymbol{\delta}\|$. ■

Remark 2. How restrictive are the assumptions $k < n$ and $\boldsymbol{\beta}_{n-k} \neq 0$? All inequality constraints are satisfied as equalities when $k = n$: either $\lambda_i = 0$ or $\mu_i = 0$ or $\lambda_i = \mu_i = 0$ for every i. As we are minimizing the distance between $\boldsymbol{\alpha}$ and $\boldsymbol{\mu}$ or $\boldsymbol{\lambda}$, λ_i is 0 only when $\mu_i = 0$ except for special cases. Hence, for $k = n$ with $\mu_i = 0$ for every i implies that the original stiffness matrix contained a row $\boldsymbol{\alpha}$ with only non-positive entries on the off-diagonal. Since $S_{ii} = -\sum_{j \neq i} \alpha_{ij} \leq 0$ in (9) this is possible only if $\alpha_{ij} = 0$ for all j which is a singular discretization. Then consider $k = 1$ with $\boldsymbol{\beta}_{n-1} = 0$ and two cases $\lambda_1 = 0$ and $\mu_1 = 0$. When $\lambda_1 = 0$ then $\lambda_j > 0, j = 2, \ldots, n$. Then $\boldsymbol{\beta}^T \boldsymbol{\lambda} = 0$ and $\boldsymbol{\lambda}$ is not feasible for interior nodes and $\mathcal{F}_i = \emptyset$. Suppose that $\mu_1 = 0$. Then $\alpha_1 \leq 0$ and $\mu_j = \alpha_j, j = 2, \ldots, n$. Since $\boldsymbol{\beta}^T \boldsymbol{\alpha} = \beta_1 \alpha_1 = -1$ in the interior, we have that $\beta_1 > 0$ but $\beta_1 \lambda_1 \geq 0$ and $\boldsymbol{\lambda}$ is not feasible. Hence, $\boldsymbol{\beta}_{n-1} \neq 0$ in the interior and the sufficient condition is satisfied when $k = 1$. ■

Suppose that $\varphi + \theta = \pi + \nu$ with $\nu > 0$ in a triangular mesh as in Fig. 1(b) in Sect. 2.2. Then the FEM jump coefficient along the edge $\mathbf{e}_{ij}$ in (10) and (13) is given by

$$\alpha_j = \gamma S_{ij}/V_j = -\gamma \sin(\nu)/(2V_j \sin(\varphi)\sin(\theta)) < 0,$$

which is small for small ν.

Since

$$\|\boldsymbol{\lambda} - \boldsymbol{\alpha}\| \leq \|\boldsymbol{\lambda} - \boldsymbol{\mu}\| + \|\boldsymbol{\mu} - \boldsymbol{\alpha}\| \leq (2 + \frac{\|\boldsymbol{\beta}_k\|}{\|\boldsymbol{\beta}_{n-k}\|})\|\boldsymbol{\delta}\|,$$

the conclusion is that small negative α_i will introduce only small changes in $\boldsymbol{\lambda}$ compared to $\boldsymbol{\alpha}$. If $\|\boldsymbol{\beta}_k\|/\|\boldsymbol{\beta}_{n-k}\|$ is large then the best choice may be to solve (51) and take $\boldsymbol{\lambda} = \boldsymbol{\mu}$.

Suitable other linear equality constraints in (50) are likely to improve the quality of $\boldsymbol{\lambda}$, too, but there may be no non-negative $\boldsymbol{\lambda}$ satisfying the extended constraints. As an example consider the consistency conditions for a FDM approximating the Laplacian. The Taylor expansion of E_j at $\mathbf{x}_j = \mathbf{x}_i + (h_{xj}, h_{yj}),\ j = 1, \ldots, n_i$, is

$$E_j = E_i + h_{xj}E_x + h_{yj}E_y + 0.5E_{xx}h_{xj}^2 + E_{xy}h_{xj}h_{yj} + 0.5E_{yy}h_{yj}^2 + \mathcal{O}\left(h_j^3\right),$$

where E_x, E_y, E_{xx}, E_{xy}, and E_{yy} are the first and second derivatives of E about $\mathbf{x}_i$ and $h_j = \max(h_{xj}, h_{yj})$. Then the consistency conditions on λ_{ij} are

$$\begin{array}{lll} \sum_j^{n_i} \lambda_{ij} h_{xj} = 0, & \sum_j^{n_i} \lambda_{ij} h_{yj} = 0, & \\ \sum_j^{n_i} \lambda_{ij} h_{xj}^2 = 2, & \sum_j^{n_i} \lambda_{ij} h_{xj} h_{yj} = 0, & \sum_j^{n_i} \lambda_{ij} h_{yj}^2 = 2, \end{array} \tag{55}$$

by requiring that $\sum_j \lambda_{ij}(E_j - E_i) = \Delta E + \mathcal{O}(h_j)$. If the number of adjacent nodes to $\mathbf{x}_i$ is three, then $n_i = 3$ in (55) and it is improbable that all five equalities can be satisfied even without imposing non-negativity on λ_{ij}. When $n_i = 4$ in a Cartesian mesh a non-negative solution exists due to the symmetry in the constraints. By adding only the first two constraints in (55), a convective part is avoided in the approximation of the Laplacian. At least one h_{xj} and one h_{yj} must have a different sign than the other ones for a solution $\boldsymbol{\lambda} \geq 0$ to exist.

4 Numerical Experiments

For the numerical experiments in 1D and 2D in this section we choose the nearest neighbors among the vertices to define ω in (15) when the local first exit times (LFET) are used to generate the jump coefficients as in Sect. 3.2. In Sect. 3.3, the diffusion coefficients are derived from the global first exit time (GFET), which we will examine in other numerical experiments in 2D. Triangular meshes in 2D are generated by COMSOL Multiphysics. The placement of nodes is manipulated manually to obtain meshes of poor quality. The solutions to (31) in LFET and PDEs for comparisons are obtained by the same software.

4.1 Local first exit times in 1D

In the following, we simulate diffusion in 1D by using the LFET from a vertex x_i. The subdomain ω, which the molecules have to leave to be recorded at the next vertex, is the interval between the neighboring vertices x_{i-1} and x_{i+1}. The interval $\Omega = [0, 1]$ is partitioned randomly into 20 subintervals with one vertex at 0.5. Then we release $M = 10^4$ molecules at $x_0 = 0.5$ at $t = 0$ with a diffusion constant $\gamma = 10^{-3}$. The distribution of the molecules at the final time $T = 20$ is found in Fig. 5(a) and a comparison is made with the solution of the mean field equation

$$\begin{aligned} \frac{\partial c(\mathbf{x}, \mathbf{x}_0, t)}{\partial t} &= \gamma \Delta c(\mathbf{x}, \mathbf{x}_0, t), \quad \mathbf{x} \in \Omega, \\ \frac{\partial c(\mathbf{x}, \mathbf{x}_0, t)}{\partial n} &= 0, \ \mathbf{x} \in \partial\Omega, \quad c(\mathbf{x}, \mathbf{x}_0, 0) = \delta(\mathbf{x} - \mathbf{x}_0). \end{aligned} \tag{56}$$

We observe that the LFET yields a good approximation of diffusion in 1D even on a very irregular mesh. This agrees with the results from section 3.2, which show that the one-dimensional first exit times reproduce the coefficients of a finite difference approximation.

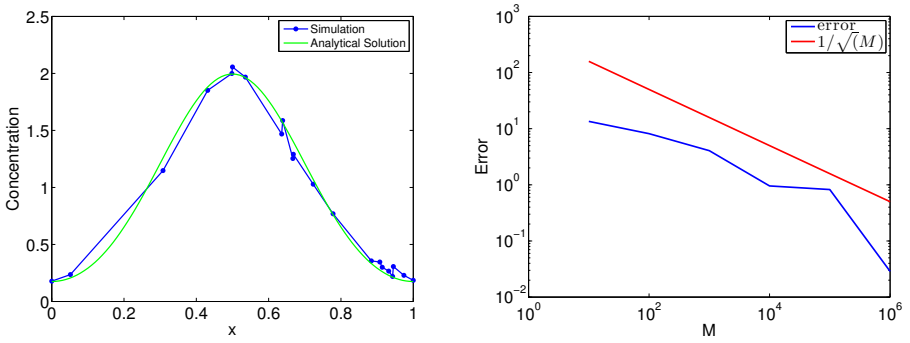

(a) (b)

Fig. 5: (a) Diffusion with $\gamma = 10^{-3}$ simulated by local first exit times for $M = 10^4$ molecules until time $T = 20$ on the interval $[0, 1]$ partitioned into $n = 21$ nodes. The vertices are marked by dots. (b) The error in the simulated exit time depending on the number of trajectories M when $L = 1, \gamma = 10^{-3}, n = 11, x_0 = 0.5$.

The error in the concentration $\tilde{c}$ from the stochastic simulation of the diffusion compared to the analytical solution c of (56) and the numerical solution c_h of (56) is known in general to behave as

$$\|c - \tilde{c}\| \leq \|c - c_h\| + \|c_h - \tilde{c}\| = \mathcal{O}(h^2) + \mathcal{O}(M^{-\frac{1}{2}}), \tag{57}$$

where h is the maximum mesh size and M is the number of molecules in the stochastic simulation. Then c_h converges to the analytical solution as h^2 with a standard FEM discretization and the stochastic simulation converges to the numerical approximation as $M^{-\frac{1}{2}}$, [30]. Convergence for $\tilde{c}$ in h is confirmed numerically in 2D for Cartesian meshes in [36] and for unstructured meshes in [11].

The convergence of the simulated exit time from the center of the interval is compared in Fig. 5(b) to the $E(x)$ satisfying (25). We discretize $[0, 1]$ with 11 equidistant vertices and release the molecules at $x_0 = 0.5$ and measure the time when they hit the boundary. The average of M trajectories is compared to the theoretical expected exit time in (26) and [44]

$$E(x_0) = \frac{1}{2\gamma} x_0(1 - x_0) = 125. \tag{58}$$

The error in Fig. 5(b) decreases as $\sim M^{-\frac{1}{2}}$ as expected for a Monte Carlo method and for the concentration in (57).

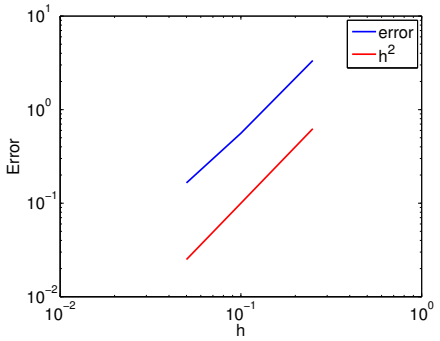

(a)

Fig. 6: Convergence of the error of the expected first exit time E in 2D for $h \to 0$ on a square with $L = 1$, $x_0 = (0.5, 0.5)$, and $\gamma = 1$, with $M = 10^7$.

On a square Ω there is a known analytical solution to the first exit time, see e.g. [36]. The jump coefficients are determined by the five point FDM stencil for the Laplacian with equidistant grid points such that $\lambda_0 = 4\gamma/h^2$ and $\bar{j}_{0i} = 1/4, i = 1, 2, 3, 4$. We compare the expected first exit time from the initial point $(0.5, 0.5)$ to $\partial\Omega$ to the solutions of stochastic simulations with $M = 10^7$. The error behaves as h^2 in Fig. 6 as is the case for the solution of the diffusion equation in (57). The error due to the Monte Carlo method is negligible here because of the large M. The discretization error $\|c - c_h\|$ in the 1D example above vanishes since the approximation in (11) solves the differential equation (25) exactly. We have shown experimentally that the error in the mean first exit time computed on a discrete mesh also satisfies a relation such as (57).

4.2 General triangular meshes in 2D

We now want to investigate the LFET and GFET on triangular meshes in 2D. The square $[-0.5, 0.5] \times [-0.5, 0.5]$ is triangulated in two meshes, one with approximately equal edge lengths and one with a perturbed area. As both meshes are of good quality and no negative entries occur in the off-diagonal elements of the diffusion matrix, the FEM and the GFET methods are identical.

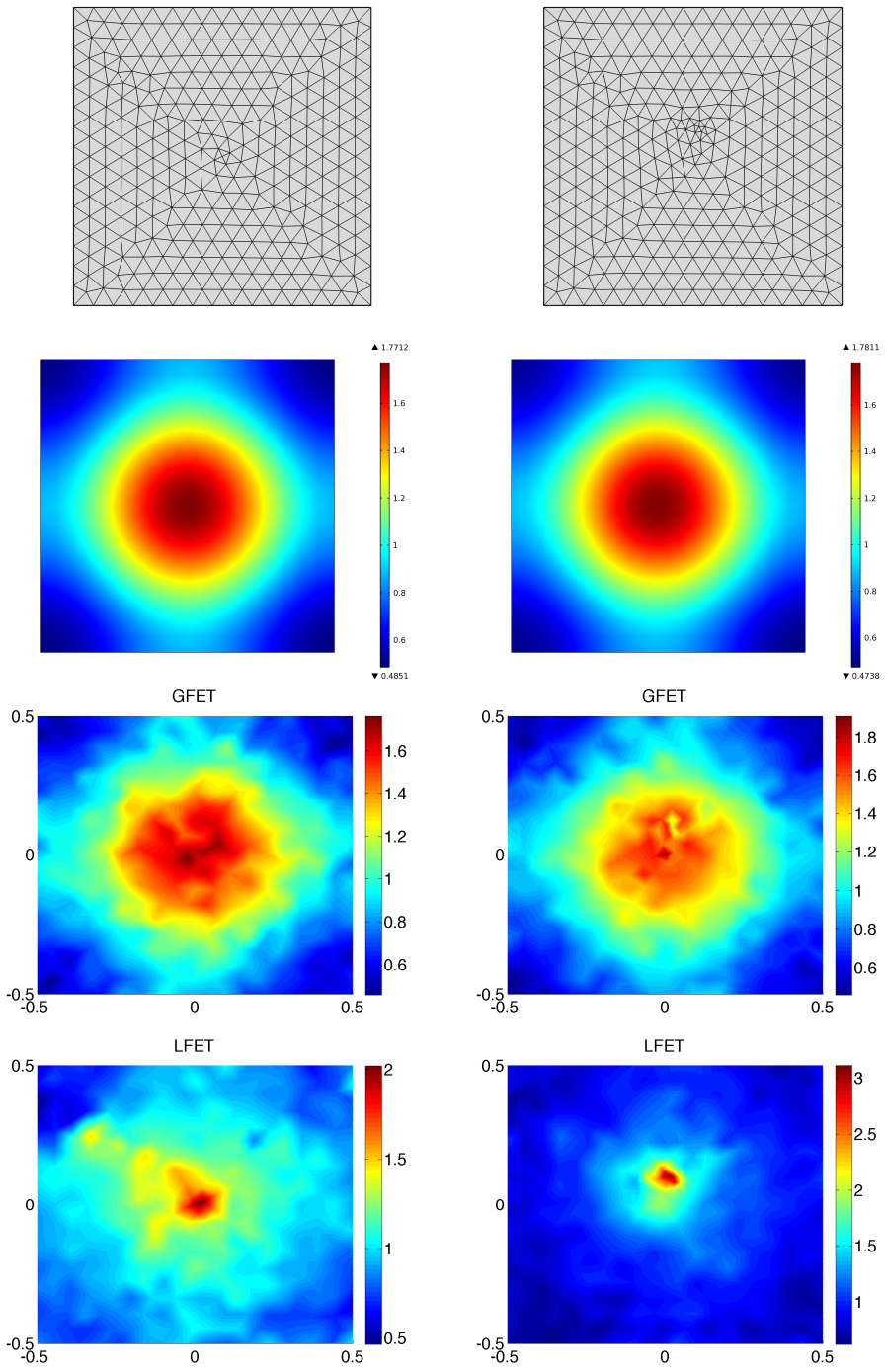

Fig. 7: Diffusion of the concentrations on the two meshes depicted in the first row with $\gamma = 10^{-3}$ until $T = 50$. The second row shows the deterministic reference solution. The third and fourth rows show the concentrations computed with the GFET and the LFET methods, respectively.

The LFET jump coefficients λ_0 and $\overline{j}_{0i}$ are determined by the procedure in Sect. 3.2. The deterministic reference solution to (56) is computed on the same meshes. The simulations in Fig. 7 are performed for $M = 10^5$ molecules initialized at the center vertex with a diffusion constant $\gamma = 10^{-3}$ until the final time $T = 50$.

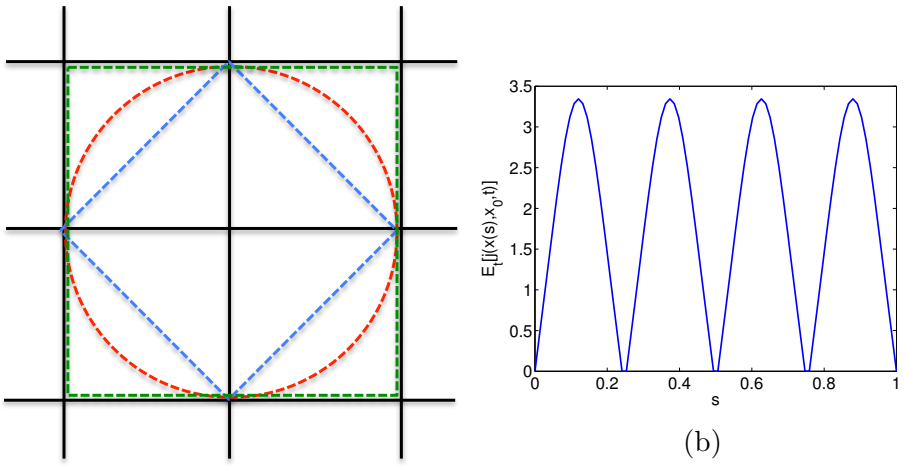

(a) (b)

Fig. 8: (a) Different ω on a Cartesian grid. (b) Expected value in time of the flux $\overline{j}_0(\mathbf{x}(s))$ out of a square starting at the midpoint.

We observe that the molecules in the LFET simulation in Fig. 7 accumulate in the smallest voxel. This phenomenon can be explained by considering a Cartesian grid. In Fig. 8, there are three different possibilities how to choose ω. Any symmetric choice of ω will have $\overline{j}_{0i} = 1/4$. The LFET approach of defining ω by the closest vertices with an edge connecting to the center vertex corresponds to the ω given by the blue line. The expected first exit time $1/\lambda_0$ from a vertex is $E = h^2/4\gamma$ on a Cartesian grid with grid size h resulting in a discretization of the Laplacian of second order accuracy [36]. This is obtained by choosing ω to be the red circle [41, p. 125],[44]. This circle covers a larger area than the blue diamond and hence the mean exit time computed from our first ω is too short. A few discretization points of $\partial\omega$ lead to a bad approximation of the boundary leading to inaccurate local first exit time approximations. The splitting probabilities between the vertices on $\partial\omega$ are the time averages of the fluxes over the edges, see (16) and (17). In Fig. 8(b), the temporal mean (16) is plotted showing the variation along a square $\partial\omega$. This variation is not resolved sufficiently well on the blue square in Fig. 8(a). There is no possibility to jump to the point with the highest probability. Moreover, the short first exit time shifts the temporal mean in

favour of the shorter jumps, which have higher probabilities for short times, see Fig. 4(b). The resolution of the boundary is improved by letting ω consist of the eight vertices marked by the green line in Fig. 8(a). A better quality of the jump coefficients is confirmed in numerical experiments in [36].

In Fig. 9, we depict a part of the right mesh in Fig. 7, where ω is defined by the colored edges and has different edge lengths between the central vertex and its neighbors. The jump propensities provided by FEM are all positive. Table 1 shows how the LFET calculates a faster jump propensity λ_0 and how this changes the distribution of jumps between the adjacent vertices. If molecules prefer to jump along the short edges they will finally accumulate in the small voxels with the short edges in the interior. Choosing the circle as ω would solve this problem on a Cartesian grid but this approach is not generalizable to unstructured meshes.

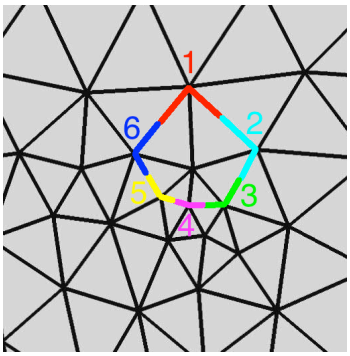

Fig. 9: Unsymmetric ω defined by the numbered vertices.

	FEM	LFET
λ	4.0655	5.5919
1	0.1379	0.1197
2	0.1777	0.1526
3	0.1584	0.1558
4	0.1947	0.2739
5	0.1588	0.1427
6	0.1725	0.1553

Table 1: Comparing the FEM and LFET on the unstructured ω in Fig. 9.

There is no guarantee that $\partial\omega$ is sufficiently well resolved for LFET on a general mesh. Therefore, we continue only with tests of the GFET approach.

4.3 Diffusion and reactions on an unstructured mesh

We examine the difference between the FEM, fulfilling (51), and the GFET, fulfilling (50). Two meshes are generated of bad quality, see in Fig. 10. Molecules of species A are released in the center node and the time when it reaches the boundary is averaged over $M = 10^5$ simulations. In Table 2 we see that the mean exit time computed by a GFET simulation converges towards the theoretical value when refining the mesh, whereas the FEM result does not seem to converge.

Theoretical value	73.6714	
No. of nodes	GFET	FEM
61	71.8534	71.5580
227	73.1575	71.8304

Table 2: Expected first exit times computed for $M = 10^5$ molecules on the meshes in Fig. 10 with the GFET and the FEM.

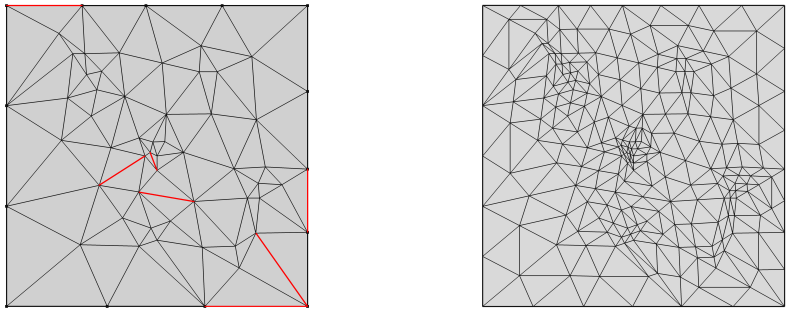

(a) (b)

Fig. 10: (a) Mesh of bad quality with 61 node. The red edges denote 14 negative coefficients. (b) Refinement of the mesh in (a) with 227 nodes and 94 negative off-diagonal entries.

To investigate the effect of the diffusion speed in a reaction system we simulate diffusion with the reaction in Table 3 on the mesh in Fig. 11 where we release $4.2 \cdot 10^5$ A molecules at the boundary $x = 0$ and equally many B molecules at the boundary $x = 2$. The quality of the mesh is better on the right hand side in Fig. 11(a) with fewer negative elements in the discretization. The SSA in Sect. 2.3 is extended as in [9, 18] to handle also the chemical reactions. The reaction parameters are scaled by the size of the voxels. The concentrations of A and B in the voxels are compared to a reference solution obtained on a high quality mesh in Fig. 12.

$$A + B \xrightarrow{k} \emptyset \quad \text{in } \Omega$$

Table 3: The parameters are $k = 5, \gamma = 10^{-3}$.

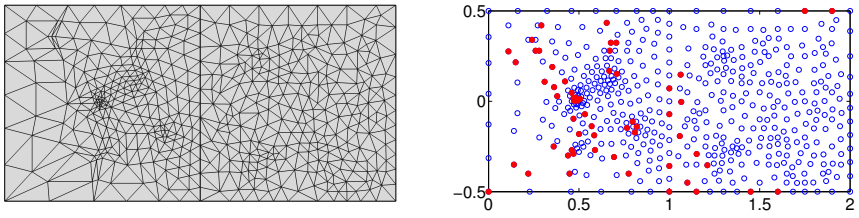

(a) (b)

Fig. 11: (a) Irregular mesh. (b) Positions of vertices (blue) and vertices with negative coefficients (red).

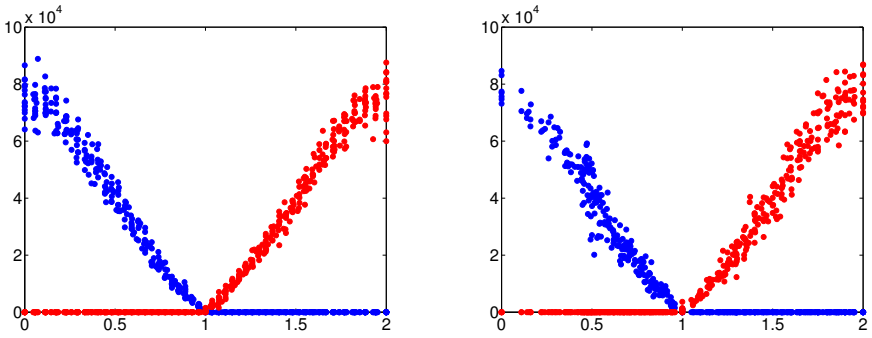

(a) (b)

Fig. 12: Concentrations of molecules along the x-axis with the reaction in Table 3 simulated until a time $T = 100$. (a) Reference solution on a regular mesh. (b) GFET simulated on the mesh in Fig. 11.

The GFET algorithm handles the bad quality of the mesh in Fig. 11 well in Fig. 12(b) and the distribution of molecules is symmetric as in the reference solution. The larger variation at $x \approx 0.5$ in Fig. 12(b) is explained by the small voxels there. The negativity of the off-diagonal elements for the mesh in Fig. 11 is small in absolute value and the FEM approach gives a qualitatively similar result.

4.4 A special triangular mesh in 2D

We consider the mesh covering the rhombus in Fig. 13 with a regularity such that the problem with negative coefficients is the same at all inner vertices.

The angles opposing an edge along the long diagonal add up to more than π and the corresponding FEM coefficients are negative (10). There is now a possibility to control the effects of bad meshes by choosing a φ. In 2D, mesh generators in general generate sufficiently good meshes, so that an evaluation of the effect of skewed triangles becomes difficult using them. In 3D, meshes often do not fulfill the quality requirements in all tetrahedra and the examination of methods based on first exit times on those meshes will be the subject of a future investigation. If not stated differently, $\varphi = 3\pi/4$ in this section.

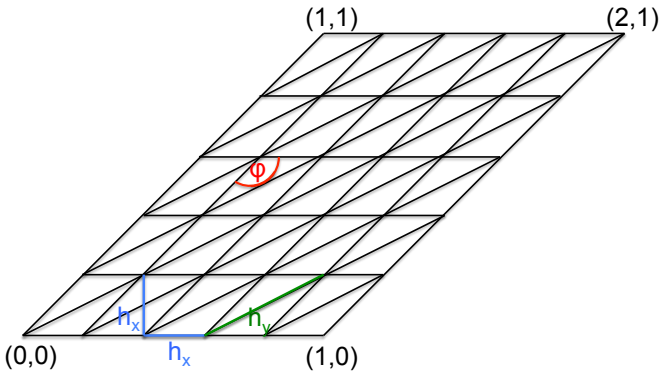

Fig. 13: Skewed mesh for $\varphi = 3\pi/4$.

Increasing φ from $\pi/2$ leads to an increasingly negative entry on the off-diagonal of the $\mathbf{D}$ matrix in (7) using the FEM, see Fig. 14. The optimization in the GFET approach with the non-negativity constraint and the equality constraint (50) finds a solution by setting the negative entry to zero and slightly changing the other entries in a row in $\mathbf{D}$, see Fig. 15.

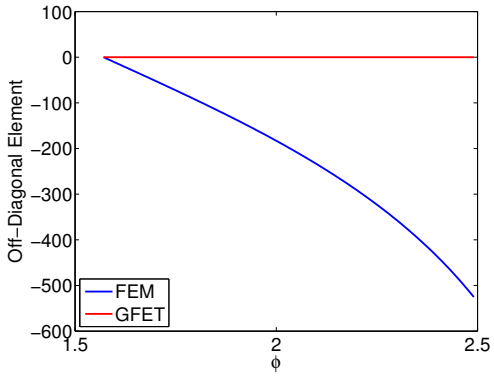

Fig. 14: Values of the jump coefficient by FEM and GFET for the edges along the long diagonal in Fig. 13 with $n_x = n_y = 21$, $h_x = 0.05$.

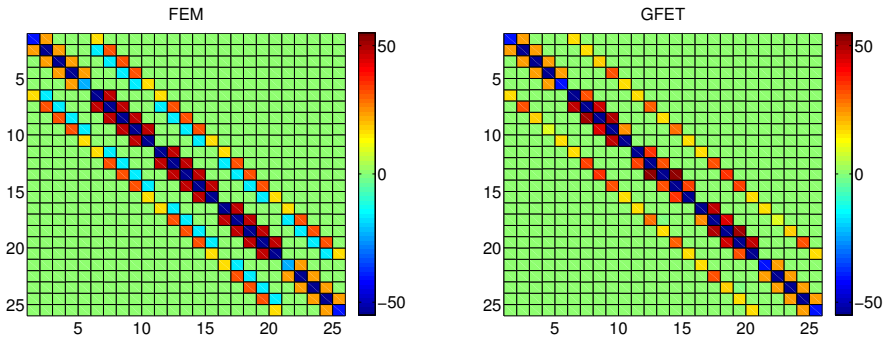

(a) (b)

Fig. 15: Jump coefficient matrices for the mesh in Fig. 13 with $\phi = 3\pi/4$ and $n_x = n_y = 5$. (a) A FEM discretization of the Laplacian. (b) After optimization with the equality constraint (GFET).

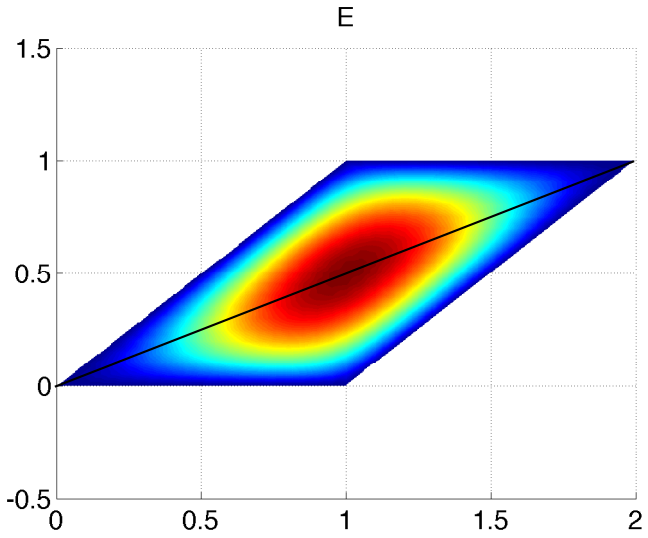

Fig. 16: Reference solution for the first exit time $E(\mathbf{x})$.

A reference solution for the expected first exit time is computed by solving (25) numerically on a fine mesh, see Fig. 16. The first exit time is recorded for a molecule starting at different vertices in the rhombus in Fig. 13 with $M = 10^4$ trajectories from each vertex. The average value approximates the expected first exit time. The first exit time is very well approximated by the GFET coefficients in (50) in Fig. 17 from an initial point along the diagonal of the rhombus in Fig. 16. The FEM coefficients in (51) result in too fast

diffusion. A similar result can be expected for a more complicated geometry containing a cavity representing the cellular nucleus for example, since (25) holds for all connected domains. It is especially on these geometries that the mesh can have bad quality and the FEM discretization gives negative coefficients.

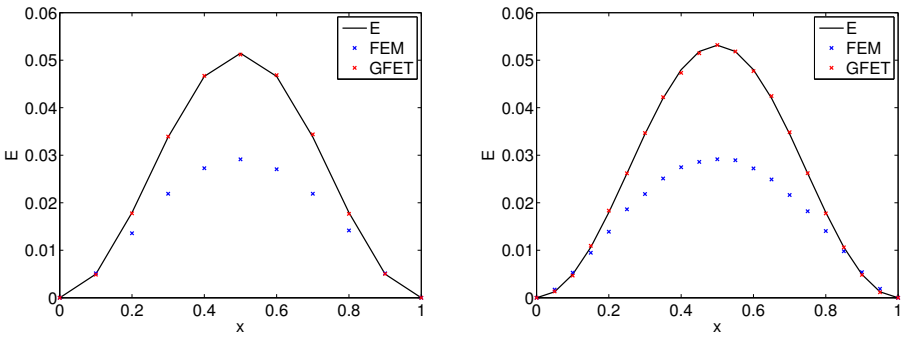

(a) (b)

Fig. 17: Expected first exit times along the diagonal in Fig. 16 calculated by the average of 10^4 FEM and GFET simulations and the computed theoretical value E on that mesh, where (a) $n_x = n_y = 11$. (b) $n_x = n_y = 21$.

The concentration determined by a stochastic simulation with FEM or GFET coefficients is compared to a computed reference solution of (56) on a fine grid in Fig. 18. Again we observe that with FEM the diffusion is too fast, whereas the GFET gives a qualitatively better solution.

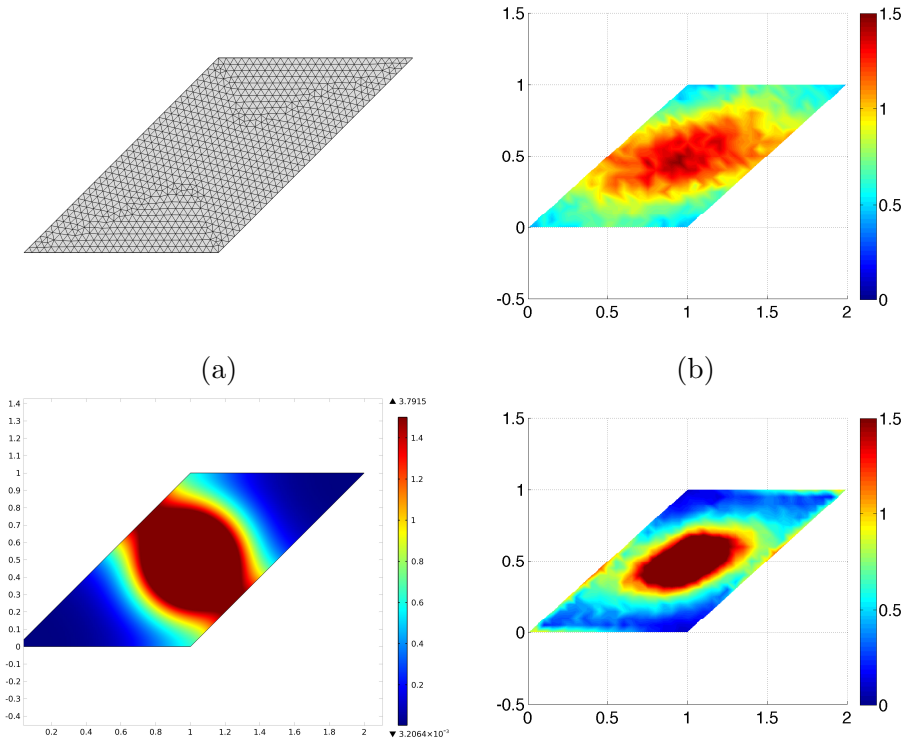

Fig. 18: Numerical simulation for $\phi = 3\pi/4$ until time $T = 0.025$ with $\gamma = 1$, $n_x = n_y = 21$ and $h_x = 0.05$ for $M = 10^5$ molecules and $x_0 = (1, 0.5)$. (a) Mesh for the numerical reference solution. (b) Stochastic simulation with FEM coefficients solving (51). (c) Numerical solution on fine mesh in (a). (d) Stochastic simulation with GFET coefficients solving (50).

The coefficients from the optimization procedure in (50) and Sect. 3.3 are inspected for this particular mesh. For the upper right and lower left corners, the right hand side η_i of (50) is negative and $E_i = 0$. All $E_j = 0$ except for the vertex with $E_j > 0$ and $\alpha_j < 0$. Hence, the optimization problem cannot be solved for a $\lambda_i > 0$ and λ is chosen as in (52). The relative difference between the original rows α of the diffusion matrix and the rows after optimization λ is found in Fig. 19. An increasing angle φ increases the difference. Furthermore, there is an increased difference in the central nodes. This can already be observed in Fig. 15 and is illustrated further in Fig. 20. Whereas the diffusion propensity out of the voxel, proportional to the diagonal entry, is constant in the FEM case it varies in space for the GFET method. The objectives of the two different ways of defining the jump coefficients are different. The aim of the GFET coefficients is to achieve the

right speed to the boundary and the aim of the unmodified FEM coefficients is to approximate the Laplacian.

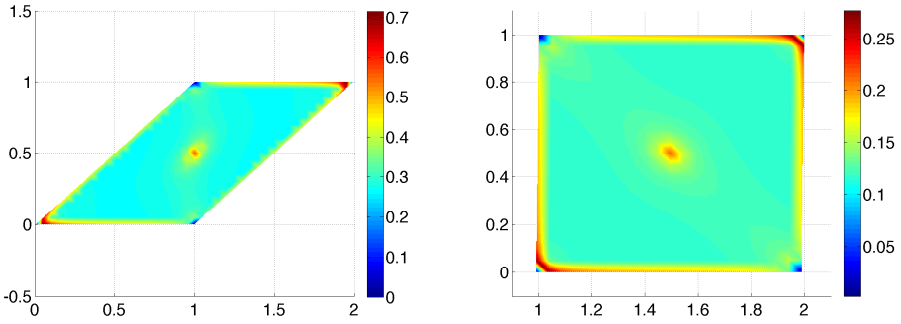

(a) (b)

Fig. 19: Relative difference $\|\lambda - \alpha\|/\|\alpha\|$ on the rhombus for $n_x = n_y = 21$ for: (a) $\phi = 3\pi/4$ and (b) $\phi = \pi/2 + 0.1$.

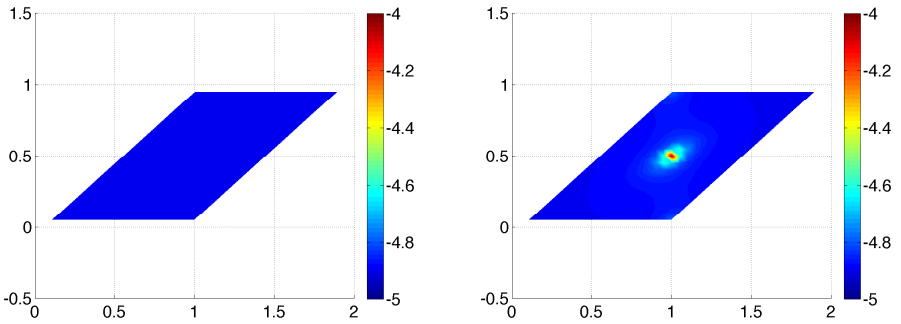

(a) (b)

Fig. 20: Diagonal elements of the diffusion matrix for (a) FEM. (b) GFET.

4.5 Boundary Reactions

The importance of the right diffusion speed is examined by simulating the system in Table 4 representing a simple signaling pathway. The signal A is created in the center of the rhombus Ω, it diffuses in the cytosol to the boundary $\partial\Omega$ where it releases protein B, which then diffuses in the cytosol and is annihilated.

$$
\begin{array}{ll}
\emptyset \xrightarrow{k_1} A & \text{at } \mathbf{x}_0 = (1, 0.5) \\
A \xrightarrow{\mu} B & \text{on } \partial\Omega \\
B \xrightarrow{k_2} \emptyset & \text{in } \Omega
\end{array}
$$

Table 4: The parameters are $k_1 = 50, k_2 = 1, \mu = 200, \gamma = 0.04$.

This reaction-diffusion system can be modelled deterministically by the PDEs for the concentrations a and b

$$
\begin{aligned}
\frac{\partial a}{\partial t} &= k_1\delta(\mathbf{x}_0) + \gamma\Delta a, \text{ in } \Omega, \quad \gamma\mathbf{n}\cdot\nabla a = -\mu a, \text{ on } \partial\Omega, \\
\frac{\partial b}{\partial t} &= -k_2 b + \gamma\Delta b, \text{ in } \Omega, \quad \gamma\mathbf{n}\cdot\nabla b = \mu a, \text{ on } \partial\Omega,
\end{aligned} \tag{59}
$$

where the normal $\mathbf{n}$ at $\partial\Omega$ is pointing out from Ω. The steady state equations for a and b are

$$
k_1\delta(\mathbf{x}_0) + \gamma\Delta a = 0, \quad -k_2 b + \gamma\Delta b = 0. \tag{60}
$$

Integrate the equations in (60) over Ω to obtain

$$
\begin{aligned}
\int_\Omega k_1\delta(\mathbf{x}_0) + \gamma\Delta a \, d\Omega &= k_1 + \gamma\int_{\partial\Omega} \mathbf{n}\cdot\nabla a \, dS = 0, \\
\int_\Omega -k_2 b + \gamma\Delta b \, d\Omega &= -k_2\int_\Omega b \, d\Omega + \gamma\int_{\partial\Omega} \mathbf{n}\cdot\nabla b \, dS = 0.
\end{aligned} \tag{61}
$$

By the boundary conditions and (61), the total amount of B at steady state is

$$
b_{tot} = \int_\Omega b \, d\Omega = \frac{\gamma}{k_2}\int_{\partial\Omega} \mathbf{n}\cdot\nabla b \, dS = \frac{\mu}{k_2}\int_{\partial\Omega} a \, dS = -\frac{\gamma}{k_2}\int_{\partial\Omega} \mathbf{n}\cdot\nabla a \, dS = \frac{k_1}{k_2}. \tag{62}
$$

To be able to solve the equation analytically for a, it is restricted to 1D. The equation in $[-\ell, \ell]$ is

$$
\frac{\partial a}{\partial t} = k_1\delta(\mathbf{x}_0) + \gamma\frac{\partial^2 a}{\partial x^2}, \quad x = -\ell : \gamma\frac{\partial a}{\partial x} = \mu a; \; x = \ell : \gamma\frac{\partial a}{\partial x} = -\mu a, \tag{63}
$$

with the stationary solution

$$
a(x) = \begin{cases} \dfrac{k_1}{2\gamma}x + \dfrac{k_1}{2}\left(\dfrac{\ell}{\gamma} + \dfrac{1}{\mu}\right), & x < 0, \\ -\dfrac{k_1}{2\gamma}x + \dfrac{k_1}{2}\left(\dfrac{\ell}{\gamma} + \dfrac{1}{\mu}\right), & x \geq 0. \end{cases} \tag{64}
$$

The total amount of A at steady state is

$$a_{tot} = \int_\Omega a \, d\Omega = \frac{k_1 \ell}{2} \left(\frac{1}{\mu} + \frac{\ell}{2\gamma} \right). \tag{65}$$

The conclusion from (62) is that the total amount of B only depends on k_1 and k_2 and from (64) and (65) that the total amount of A depends on the diffusion constant. A high diffusion constant γ results in a lower concentration of A molecules and vice versa. In Fig. 21, we present the simulation of the system in Table 4 with the FEM and the GFET methods and a reference solution on a mesh without negative coefficients in Fig. 22. The GFET agrees very well with the reference solution. The FEM, with too fast diffusion corresponding to a larger γ, results in a lower concentration of A molecules, which agrees qualitatively with what is expected from the solution of the steady state equation (64) and (65) in 1D. The concentration of species B is not affected by the diffusion speed and is close to k_1/k_2 after the transient phase as in (62).

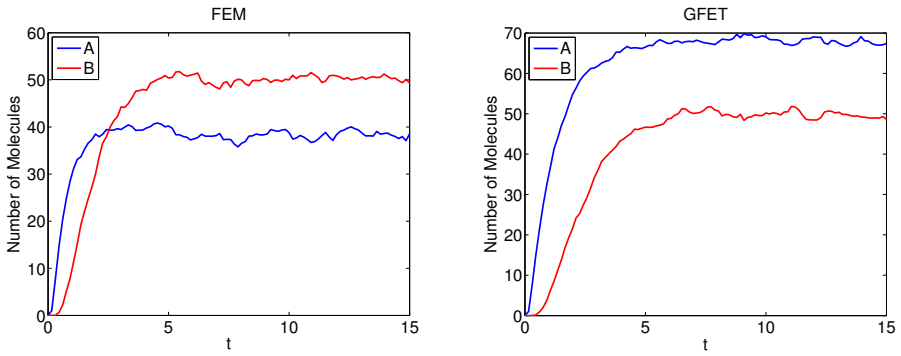

(a) (b)

Fig. 21: Average of 50 simulations of the system in Table 4 simulated on the mesh in Fig. 13 with $n_x = n_y = 21$ until time $T = 15$. (a) FEM. (b) GFET.

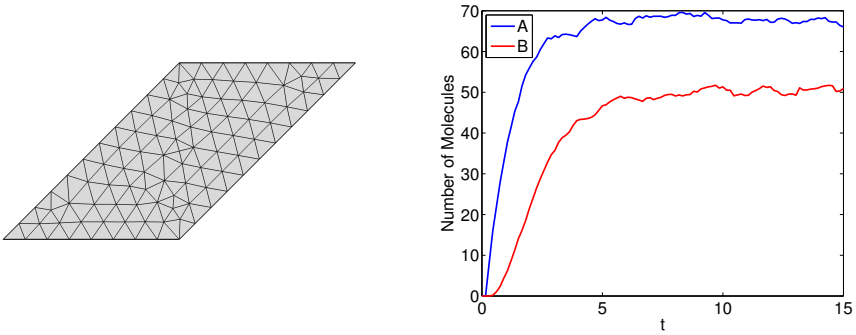

(a) (b)

Fig. 22: (a) Reference grid. (b) Average of 50 simulations of the system in Table 4 simulated on the grid in (a) until time $T = 15$.

The expected first exit time in Fig. 17 depends on the diffusion as $E \sim 1/\gamma$ and the quotient q between the maxima of E with FEM and GFET is about 0.55 in Fig. 17. It follows from (65) with a large μ that $a_{tot} \sim 1/\gamma$. In Fig. 21, the quotient between a_{tot} with FEM and GFET is about $40/70 \approx 0.57$. An interpretation of the FEM coefficients is that they represent diffusion with a higher coefficient γ, about 1.8 times larger, in these two cases.

5 Conclusion

We have applied the theory of first exit times in stochastic diffusion to derive jump coefficients in a spatial domain discretized by an unstructured mesh. The theory is applied locally (LFET) and globally (GFET). The methods are compared to diffusion simulated with the coefficients obtained from a finite element method (FEM).

The FEM coefficients approximate the Laplacian and are positive on a high quality mesh. However, sometimes in 2D and more often in 3D, mesh generators produce skewed meshes yielding negative jump coefficients with FEM. This is avoided with LFET and GFET: the coefficients are non-negative but the they do not approximate the Laplacian to second order accuracy anymore. It is probably impossible to combine linearity (in the sense that the coefficients are independent of the solution), non-negative coefficients (ensuring that the discrete maximum principle is satisfied for the Laplace equation), and a consistent approximation of the Laplacian on a general unstructured mesh. Therefore, we abandon the consistency and replace it by conditions based on the first exit time.

In the numerical experiments, the coefficients derived by LFET are found

to be sensitive to the geometry of the triangles in 2D with a lack of robustness resulting in too fast diffusion. The definition of the local domain around a vertex is critical when the vertex is surrounded by only a few other vertices.

By using the first exit time from the whole domain of interest, GFET coefficients are computed by projecting the FEM coefficients on the subspace with non-negative solutions satisfying a first exit time constraint locally. If the original FEM coefficients are non-negative then the GFET and the FEM coefficients are identical. Then in numerical experiments on a skewed mesh, the expected first exit times determined by simulations are compared to the computed solution of a PDE with good agreement. Finally, the number of molecules in an example with diffusion and reactions agrees well with mean field theory.

Acknowledgment

This work has been supported by the Swedish Research Council. We want to thank Stefan Engblom and Andreas Hellander for their helpful comments on this work.

References

[1] S. S. Andrews, N. J. Addy, R. Brent, and A. P. Arkin. Detailed simulations of cell biology with Smoldyn 2.1. *PLoS Comput. Biol.*, 6(3):e1000705, 2010.

[2] J. Brandts, S. Korotov, M. Křížek, and J. Šolc. On nonobtuse simplicial partitions. *SIAM Rev.*, 51(2):317–335, 2009.

[3] L. Breiman. *Probability*. SIAM, Philadelphia, PA, 1992.

[4] E. Burman and A. Ern. Stabilized Galerkin approximation of convection-diffusion-reaction equations: Discrete maximum principle and convergence. *Math. Comp.*, 74:1637–1652, 2005.

[5] Y. Cao, D. T. Gillespie, and L. R. Petzold. The slow-scale stochastic simulation algorithm. *J. Chem. Phys.*, 122:014116, 2005.

[6] G. Dahlquist and Å. Björck. *Numerical Methods*. Prentice-Hall, Englewood Cliffs, NJ, 1974.

[7] A. Donev, V. V. Bulatov, T. Oppelstrup, G. H. Gilmer, B. Sadigh, and M. H. Kalos. A first-passage kinetic Monte Carlo algorithm for complex diffusion-reaction systems. *J. Comput. Phys.*, 229:3214–3236, 2010.

[8] B. Drawert, S. Engblom, and A. Hellander. URDME: a modular framework for stochastic simulation of reaction-transport processes in complex geometries. *BMC Syst. Biol.*, 6:76, 2012.

[9] J. Elf and M. Ehrenberg. Spontaneous separation of bi-stable biochemical systems into spatial domains of opposite phases. *Syst. Biol.*, 1:230–236, 2004.

[10] M. B. Elowitz, A. J. Levine, E. D. Siggia, and P. S. Swain. Stochastic gene expression in a single cell. *Science*, 297:1183–1186, 2002.

[11] S. Engblom, L. Ferm, A. Hellander, and P. Lötstedt. Simulation of stochastic reaction-diffusion processes on unstructured meshes. *SIAM J. Sci. Comput.*, 31:1774–1797, 2009.

[12] D. Eppstein, J. M. Sullivan, and A. Üngör. Tiling space and slabs with acute tetrahedra. *Comput. Geom.*, 27:237–255, 2004.

[13] H. Erten and A. Üngör. Quality triangulations with locally optimal Steiner points. *SIAM J. Sci. Comput.*, 31:2103–2130, 2009.

[14] L. Ferm, P. Lötstedt, and A. Hellander. A hierarchy of approximations of the master equation scaled by a size parameter. *J. Sci. Comput.*, 34:127–151, 2008.

[15] C. W. Gardiner. *Handbook of Stochastic Methods*. Springer Series in Synergetics. Springer-Verlag, Berlin, 3rd edition, 2004.

[16] C. W. Gardiner, K. J. McNeil, D. F. Walls, and I. S. Matheson. Correlations in stochastic theories of chemical reactions. *J. Stat. Phys.*, 14(4):307–331, 1976.

[17] M. A. Gibson and J. Bruck. Efficient exact stochastic simulation of chemical systems with many species and many channels. *J. Phys. Chem.*, 104(9):1876–1889, 2000.

[18] D. T. Gillespie. A general method for numerically simulating the stochastic time evolution of coupled chemical reactions. *J. Comput. Phys.*, 22(4):403–434, 1976.

[19] D. T. Gillespie and E. Seitaridou. *Simple Brownian Diffusion*. Oxford University Press, Oxford, 2013.

[20] J. Hattne, D. Fange, and J. Elf. Stochastic reaction-diffusion simulation with MesoRD. *Bioinformatics*, 21:2923–2924, 2005.

[21] I. Hepburn, W. Chen, S. Wils, and E. De Schutter. STEPS: efficient simulation of stochastic reaction-diffusion models in realistic morphologies. *BMC Syst. Biol.*, 6:36, 2012.

[22] S. A. Isaacson and C. S. Peskin. Incorporating diffusion in complex geometries into stochastic chemical kinetics simulations. *SIAM J. Sci. Comput.*, 28(1):47–74, 2006.

[23] T. Jahnke and W. Huisinga. Solving the chemical master equation for monomolecular reaction systems analytically. *J. Math. Biol.*, 54(1):1–26, 2007.

[24] N. G. van Kampen. *Stochastic Processes in Physics and Chemistry*. Elsevier, Amsterdam, 5th edition, 2004.

[25] E. Keilegavlen, J. M. Nordbotten, and I. Aavatsmark. Sufficient criteria are necessary for monotone control volume methods. *Appl. Math. Lett.*, 22:1178–1180, 2009.

[26] R. A. Kerr, T. M. Bartol, B. Kaminsky, M. Dittrich, J.-C. J. Chang, S. B. Baden, T. J. Sejnowski, and J. R. Stiles. Fast Monte Carlo simulation methods for biological reaction-diffusion systems in solution and on surfaces. *SIAM J. Sci. Comput.*, 30(6):3126–3149, 2008.

[27] E. Kieri. Accurracy aspects of the reaction-diffusion master equation on unstructured meshes. Technical Report MSc thesis, UPTEC F 11014, Uppsala University, Uppsala, Sweden, 2011.

[28] S. Korotov, M. Křížek, and P. Neittanmäki. Weakened acute type condition for tetrahedral triangulations and the discrete maximum principle. *Math. Comp.*, 70:107–119, 2000.

[29] T. G. Kurtz. Solutions of ordinary differential equations as limits of pure jump Markov processes. *J. Appl. Prob.*, 7:49–58, 1970.

[30] T. G. Kurtz. Limit theorems for sequences of jump Markov processes approximating ordinary differential processes. *J. Appl. Prob.*, 8:344–356, 1971.

[31] K. Lipnikov, D. Svyatskiy, and Y. Vassilevski. A monotone finite volume scheme for advection-diffusion equations on unstructured polygonal meshes. *J. Comput. Phys.*, 229:4017–4032, 2010.

[32] P. Lötstedt. Perturbation bounds for the linear least squares problem subject to linear inequality constraints. *BIT*, 23:500–519, 1984.

[33] A. J. Mauro, J. K. Sigurdsson, J. Shrake, P. J. Atzberger, and S. A. Isaacson. A First-Passage Kinetic Monte Carlo method for reaction-drift-diffusion processes. *J. Comput. Phys.*, 259:536–567, 2014.

[34] H. H. McAdams and A. Arkin. Stochastic mechanisms in gene expression. *Proc. Natl. Acad. Sci. USA*, 94:814–819, 1997.

[35] D. A. McQuarrie. Stochastic approach to chemical kinetics. *J. Appl. Prob.*, 4:413–478, 1967.

[36] L. Meinecke and P. Lötstedt. Stochastic diffusion processes on Cartesian meshes. Technical Report 2013-022, Dept. of Information Technology, Uppsala University, Uppsala, Sweden, 2013. Available at `http://www.it.uu.se/research/publications/reports/`.

[37] R. Metzler. The future is noisy: The role of spatial fluctuations in genetic switching. *Phys. Rev. Lett.*, 87:068103, 2001.

[38] I. D. Mishev. Finite volume methods for Voronoi meshes. *Num. Meth. Part. Diff. Eq.*, 54(2):193–212, 1998.

[39] B. Munsky, G. Neuert, and A. van Oudenaarden. Using gene expression noise to understand gene regulation. *Science*, 336(6078):183–187, 2012.

[40] K. B. Nakshatrala and A. J. Valocchi. Non-negative mixed finite element formulations for a tensorial diffusion equation. *J. Comput. Phys.*, 228:6726–6752, 2009.

[41] B. Øksendal. *Stochastic Differential Equations*. Springer, Berlin, 6th edition, 2003.

[42] T. Oppelstrup, V. V. Bulatov, A. Donev, M. H. Kalos, G. H. Gilmer, and B. Sadigh. First-passage kinetic Monte Carlo method. *Phys. Rev. E*, 80:066701, 2009.

[43] A. Raj and A. van Oudenaarden. Nature, nurture, or chance: Stochastic gene expression and its consequences. *Cell*, 135(2):216–226, 2008.

[44] S. Redner. *A Guide to First-Passage Processes*. Cambridge University Press, Cambridge, 2001.

[45] Z. Sheng and G. Yuan. An improved monotone finite volume scheme for diffusion equation on polygonal meshes. *J. Comput. Phys.*, 231:3739–3754, 2012.

[46] P. S. Swain, M. B. Elowitz, and E. D. Siggia. Intrinsic and extrinsic contributions to stochasticity in gene expression. *Proc. Natl. Acad. Sci. USA*, 99(20):12795–12800, 2002.

[47] K. Takahashi, S. Tănase-Nicola, and P. R. ten Wolde. Spatio-temporal correlations can drastically change the response of a MAPK pathway. *Proc. Natl. Acad. Sci. USA*, 107(6):2473–2478, 2010.

[48] V. Thomée and L. Wahlbin. On the existence of maximum principles in parabolic finite element equations. *Math. Comp.*, 77:11–19, 2008.

[49] R. S. Varga. *Matrix Iterative Analysis*. Prentice-Hall, Englewood Cliffs, NJ, 1962.

[50] J. Xu and L. Zikatanov. A monotone finite element scheme for convection-diffusion equations. *Math. Comp.*, 68:1429–1446, 1999.

[51] C. A. Yates and R. E. Baker. Importance of the Voronoi domain partition for position-jump reaction-diffusion processes on nonuniform rectilinear lattices. *Phys. Rev. E*, 88:054701, 2013.

[52] J. S. van Zon and P. R. ten Wolde. Green's-function reaction dynamics: A particle-based approach for simulating biochemical networks in time and space. *J. Chem. Phys.*, 123:234910, 2005.